5-11-2013

Sulfonated Polyethersulfone as a New Platform for Thin Film Composite Membranes

Brendan R. O'Grady
University of Connecticut - Storrs, brendan.ogrady06@gmail.com

Sulfonated Polyethersulfone as a New Platform for Thin Film Composite Membranes

Brendan Richard O'Grady

B.S., University of Connecticut, 2011

A Thesis

Submitted in Partial Fulfillment of the

Requirements for the Degree of

Master of Science

At the

University of Connecticut

2013

APPROVAL PAGE

Master of Science Thesis

Sulfonated Polyethersulfone as a New Platform for Thin Film Composite Membranes

Presented by

Brendan Richard O'Grady, B.S.

Major Advisor_____
Dr. Jeffrey R. McCutcheon

Associate Advisor_____
Dr. Leslie Shor

Associate Advisor_____
Dr. Chris Cornelius

University of Connecticut

2013

Acknowledgements

Foremost, I would like to express my sincere gratitude to my advisor Dr. Jeffrey McCutcheon for the continuous support of my M.S. study and research, for his constant support, motivation, patience, and knowledge. He was very helpful in all aspects, and I greatly appreciate the time he spent advising me during both my undergraduate and graduate careers at the University of Connecticut.

Additionally, I would like to thank my fellow lab mates in the Sustainable Water and Energy Learning Lab (SWELL) for their unvarying help and support throughout all the stages of this project. Their being part of my life over the past couple years has made my time in graduate school more enjoyable. Finally, I am thankful for the support of my family who were always at my side.

Finally, I thank Solvay Specialty Polymers (Alpharetta, GA) for providing materials and funding, and both 3M (Meriden, CT) and Hydration Technologies Inc. (Albany, OR) for supplying membrane materials used in this study.

Table of Contents

1. Abstract

Membrane based separations are widely in many technically and commercially relevant processes, including sea and brackish water desalination and treatment. Current drawbacks from membrane-based processes are fouling propensity and low water fluxes. One solution to remediate these issues is the use of intrinsically hydrophilic support layers in composite membranes. The hydrophilic nature of the substrates will facilitate increased water transport across the membrane and provide anti-fouling characteristics.

This study investigated the use of sulfonated polyethersulfone (SPES) as a new material for thin film composite membranes. Four degrees of sulfonation were examined. Asymmetric membranes were cast with polymer loadings between 12-20 % by weight using n-methyl-2-pyrrolidone (NMP) as the solvent and precipitated in water. Membranes films were characterized using a variety of techniques to analyze the physical, chemical and thermal properties. Select polymers were interfacially polymerized using m-phenylenediamine (MPD) and 1,3,5-benzenetricarbonyltrichloride (TMC) to create a polyamide layer on top of the membrane supports. The thin-film composite membranes were tested in both reverse osmosis (RO) and forward osmosis (FO) systems. The sulfonated polymers on average performed just as well or better than the unmodified polyethersulfone (PES) polymer in RO applications. With respect to the FO testing, wetting negatively affected the performance of the SPES. The base PES exhibited much greater fluxes and wetting than the SPES. It was determined that sulfonated polymers are a promising new material for thin film composite membranes, particularly for RO applications.

2. List of Figures

3. Introduction

With the synthesis of many new polymers in the last decades, polymeric membranes have become an integral part of application and process development. One area of significant growth has been water treatment and purification. Membrane based processes can be utilized in every step of water treatment and purification, with reverse osmosis (RO) being the most evident for desalination. With our constant growth in industry, agriculture, and population the worldwide water demand is ever increasing. In order to accommodate these needs water treatment and purification methods must be as energy and cost effective as possible [1, 3, 4]. Therefore, the polymeric membranes utilized in these processes have to be efficient. Much time and effort have gone into the development of specific polymers for membranes; one promising polymer is sulfonated polyethersulfone (SPES). Polyethersulfone (PES) is a very common polymer used in commercial membrane fabrication. SPES is a modified PES in that there are sulfonic acid group located orthogonally to the ether on the aryl groups.

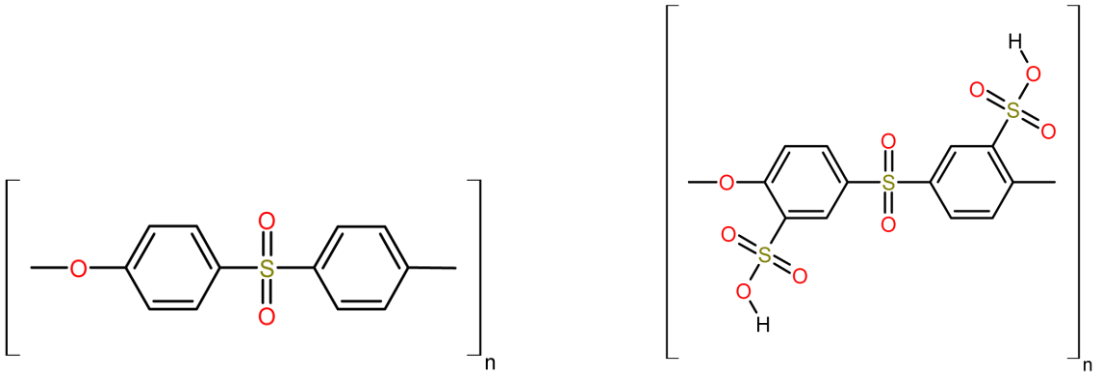

Figure 1: Chemical structures of polyethersulfone (PES, Left) and Sulfonated Polyethersulfone (SPES, Right).

3.1. Membrane Based Water Treatment Processes

Separations by the use of membranes are becoming increasingly more significant in industrial processes, especially as water becomes a more vital resource. Membranes act as a semipermeable barrier and separation occurs by the membrane controlling the rate of

movement of various molecules between two phases, albeit both liquid, both gas, or a liquid and a gas. The most important property of membranes is their ability to control the rate of permeation of different species [1].

There are many different types of membranes used in industry. Some of the most prominent technologies to utilize the separation properties of membranes are water purification, gas permeation and separation, dialysis, and distillation among many others. The following figure gives a brief over-view of some membrane applications used for liquid separations.

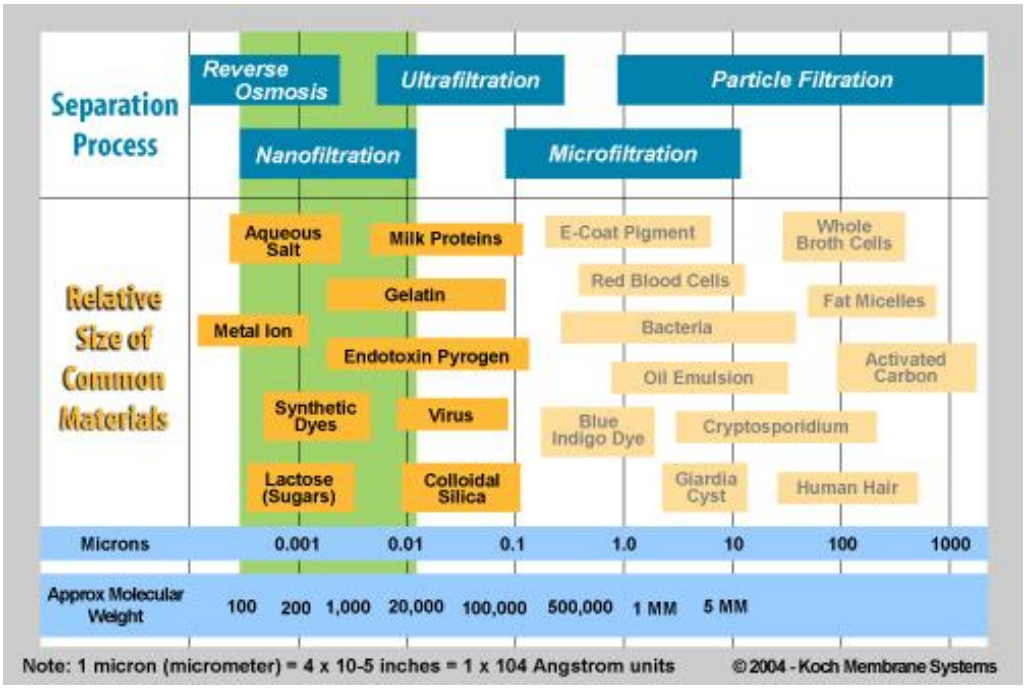

Figure 2: Table comparing various membrane separation methods and particle rejection size [2].

As shown in Figure 2 there are several different membrane processes. Let it be known that the processes in Figure 2 are all water separation methods. The primary differences between the processes are the pore size and molecular cutoff weights. Of the processes listed, reverse osmosis (RO), Nanofiltration (NF), Ultrafiltration (UF), and Microfiltration (MF); RO is the most selective, in that the pore size and molecular cutoff weights are the smallest,

whereas MF is the least selective and therefore has the largest pore size and molecular cut-off weight.

As mentioned previously, water is of the utmost importance, especially in a time when the population is growing rapidly, and people's needs are changing constantly. Water conservation and recycling are critical priorities, along with better water management in order to optimize water usage, minimize the water footprint and to lower the overall cost of manufacturing.

For the purpose of this paper, membrane separations will be separated into two distinct categories based upon driving force. The first category utilizes hydraulic pressure as the driving force; these processes include all of those mentioned above in Figure 2, and for all intensive purposes will be referred to as RO for the remainder of the paper**.**

The second category operates under the influence of a concentration gradient; this method is known as forward osmosis (FO). There exists another mode aptly named pressure retarded osmosis (PRO) in which the system operates in a regime that is governed by both a hydraulic and a concentration gradient, as depicted in Figure 3.

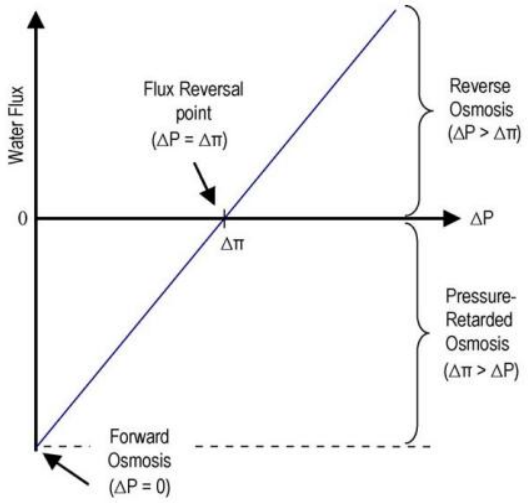

Figure 3: Water flux direction and magnitude as a function of pressure for RO, PRO, and FO [11].

The two membrane processes here FO and PRO can be combined to define the available techniques for engineered osmosis (EO) [4] and can be further seen above in Figure 3 as existing below the flux reverse point ($\Delta P = \Delta\pi$). Further discussion of both RO and FO processes are in the next section.

3.1.1. Pressure Driven Membrane Processes

In pressure driven processes, the driving force is hydraulic pressure. Depending upon the size and number of the solutes in the feed water the driving force may be greater, from Figure 2 above, it can be seen that pore size decreases as the size of solutes decreases therefore requiring a greater driving force in order to transport water through the smaller pores. Additionally, the hydraulic pressure is necessary to overcome the osmotic pressure of the feed created by the dissolved solutes. This as can be imagined is an extremely energy intensive process. One-way around this, instead of going against the nature of osmosis (reverse osmosis), we can go with osmosis, using EO processes (FO and PRO). A driving force can be engineered chemically based upon concentration (chemical potential) differences between solutions [5].

3.1.2. Osmotically Driven Membrane Processes

Engineered Osmosis (EO) processes utilize osmotic pressure gradients, these are forward osmosis (FO) and pressure retarded osmosis (PRO). Forward osmosis is a process that utilizes an engineered driving force through chemical potential differences, manifested as osmotic pressure. The osmotic pressure (π) relates to the total dissolved solids content of a solution, as described by the modified Van't Hoff equation:

$$\pi = iCRT$$

where i is the Van't Hoff factor, dissociation value of the solute in solution (i=2 for NaCl), C is the molarity of the solute in solution, R is the universal gas constant, and T is the absolute temperature of the solution.

Forward and pressure retarded osmosis, FO and PRO respectively, use osmotic pressure as their driving force. In these processes, a solution with a high osmotic pressure, called the draw solution, is on one side of the membrane, while the other side is in contact with a lower-osmotic feed solution. The feed solution is the same as in reverse osmosis, the stream treated for solute separation. Water is drawn from the feed solution into the draw solution, therefore diluting the draw solution and concentrating the feed solution. The flow of water in this instance is in the same direction as osmosis, therefore in the opposite direction of reverse osmosis. PRO works on the same principle except that a hydraulic pressure is applied to the draw solution such that a pressurized stream is output, which can then be pushed through a turbine in order to generate electricity [6-9]. Since osmotic pressure is determined by total dissolved solids and not the specific identities of the dissolved solids this allows for the draw solution to contain solutes of an entirely different composition in order to generate a desired driving force. As a result, through the natural phenomena of osmosis, water is drawn through the membrane from the feed to the draw solution in order to equate the osmotic pressure in both solutions. The then diluted draw solution is sent to a secondary separation unit to recover the draw solute.

Despite the advantages of EO processes, they are not yet commercially relevant, with the major obstacle being the lack of suitable membranes. Thin film composite (TFC) NF and RO membranes, some of the best membranes available, are not fit for EO processes due to their dense support layers which result in limited solute mass transfer, more commonly known as internal concentration polarization (ICP) [10-14]. ICP negatively affects performance by

lowering the overall osmotic pressure gradient and therefore the driving force across the membrane [10].

3.2. Types of membranes

3.2.1. Integrated Asymmetric Membranes

Asymmetric membranes are composed of a porous support layer and an integrated dense top layer or skin. The thin top layer determines virtually all of the mass transfer resistance. Mulder describes the thickness of the skin layer on the order of magnitude of 0.1-0.5 μm while the thickness of the porous support layer ranges from 50-150 μm [15] and sometimes even greater depending on the end application. The advantage of asymmetric membranes is their high permeation rates coupled with high selectivity.

3.2.2. Thin Film Composite Membranes

Composite membranes are essentially the same except with an additional skin layer. The advantage to this design is that the top (skin) and support layers can be of different materials, therefore allowing for the independent optimization of each layer in order to obtain the best performance with respect to selectivity, permeability, chemical, mechanical and thermal stability [15].

The additional skin layer, often referred to as the active layer, where the separation occurs, is typically added using a process called interfacial polymerization. A more thorough discussion of interfacial polymerization will be later on.

3.3. Challenges with Membrane Design

The primary challenge with membrane design is overcoming the many resistances within the membrane to generate higher water fluxes. As illustrated below in Figure 4 six separate resistances need to be overcome for transport to occur through the membrane. Due to the large resistance encountered by water transporting through the membrane it is hesitant to pass

through the membrane. Decreasing the specific resistances, especially R_5, can be accomplished by utilizing different membrane materials. It has been proven previously, that transport across the active layer is diffusion dependent and not limited by the thickness of the active layer (i.e. R_2, R_3, R_4) [16].

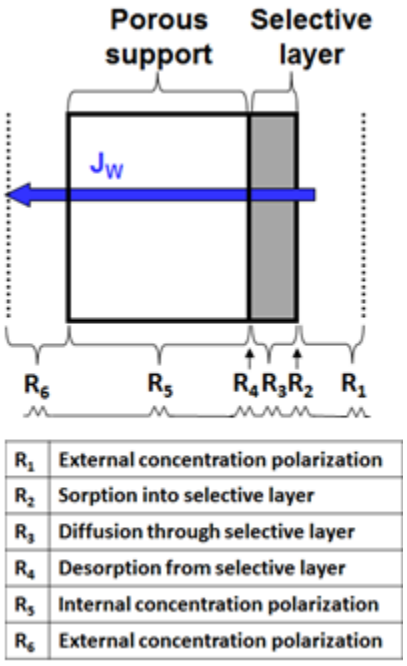

R_1	External concentration polarization
R_2	Sorption into selective layer
R_3	Diffusion through selective layer
R_4	Desorption from selective layer
R_5	Internal concentration polarization
R_6	External concentration polarization

Figure 4: Resistance profile in TFC membranes [17].

Yip [18] developed new methods for fabricating high flux FO membranes by minimizing support layer resistance. These membranes include finger-like pores that span the length of the support layer. Above them is a very thin spongy dense layer that holds the active layer. The bottoms of the membranes require an open porous layer that permits wetting. Tiraferri et al. analyzed support layer formation and structure to the performance of TFC-FO membranes [19]. In general it was determined that both active and support layer transport properties need to be optimized for the best performance.

Overall, the challenge is looking for a new platform for osmosis specific membranes, which will work in both RO and FO operating regimes. Development of thin, highly porous,

non-tortuous, and hydrophilic supports layers in order to reduce internal resistances, while also providing the permselectivity for most solutes and high water fluxes. For FO applications, it is necessary to reduce the same resistances in order to fully wet out the membrane support layer to reduce internal concentration polarization and ultimately maximize flux [20-22].

3.4. Objective

The primary objective of the study is to determine if SPES is a good candidate for support layer manufacturing for osmotic based separations. This will be ascertained by characterizing PES and SPES asymmetric membranes (support layer) to determine the effects of the added side groups, $-SO_3H$ (sulfonic acid), on the polymer properties and performance. Following the support layer characterization, interfacial polymerization will be done on select asymmetric films to make TFC membranes that will ultimately be tested in both RO and FO processes.

Few studies have been completed on the use of post-sulfonated PES as a support layer for TFC membranes for use in RO and FO processes. Brousse first began to look at sulfonated aromatic polysulfones as a new material for RO membranes because of the number of inconveniences cellulose acetate (CA) presented, specifically its great susceptibility to chemical and bacteriological agents. Furthermore, the fragility of CA creates numerous difficulties for large-scale water treatment by requiring costly pretreatment steps, in addition to storage and cleaning limitations [23]. Recently, much attention has been given to the structure and optimal reaction conditions for controlling the degree of sulfonation and not on specific application performance. Several studies have used SPES for ion exchange membranes and ultimately proved that ion exchange capacity was very good in addition to permeability, however drawbacks are swelling and low power densities for fuel cell applications [24-27].

Kim et al. prepared UF membranes by phase inversion from SPES and investigated the effects of dichloromethane and poly (vinyl pyrrolidinone) additions to the membrane casting solution on flux and salt rejection performance [28]. Overall, it was determined the negatively charged SPES reduced protein fouling and that there is a tradeoff between flux and solute rejection with increased sulfonation. Ghosh et al. reported SPES NF membranes provided superior flux and solute separation for different inorganic salts in the presence of multivalent cations when compared to PES membranes under similar conditions [29]. Furthermore, Unnikrishnan noted that both storage modulus and glass transition temperature (Tg) increase with sulfonation [30].

4. Theory

4.1. Membrane Formation

The mechanism by which a polymer precipitates from solution plays a major role in defining the resulting morphology and ultimately the transport properties [58]. Membrane formation is generally described qualitatively using a ternary phase diagram as seen in Figure 5**.**

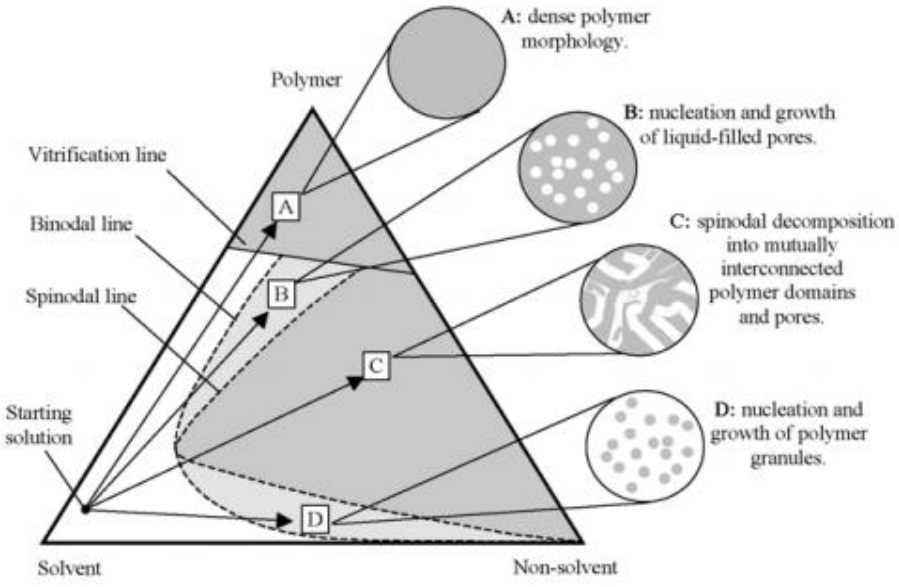

Figure 5: Phase diagram for hypothetical polymer, solvent, and nonsolvent system showing four coagulation scenarios and their resulting morphologies [58].

The ternary phase diagram illustrates the path the casted film takes during formation. The starting solution is represented on the left hand side of the diagram. As more nonsolvent is introduced into the system the film chooses a thermodynamically favorable path for film formation as it moves to the right in the diagram. If path A is followed, then vitrification will occur and a dense polymer morphology is created; whereas, pathways B and D represent binodal decomposition resulting in the nucleation and growth of pores and granules, respectively. The B pathway will result in a more polymer rich film that has more open pores rather than D that will be a polymer lean phase with a granulated structure [58]. Pathway C is the most desired for an open porous support layer that will produce the least amount of resistance to transport through the membrane. The difficulty with pathway C is that spinodal decomposition occurs with travel through the critical point (where binodal and spinodal curves meet) and is most feasible with low polymer concentrations, but the chances of defects in the film increase with lower polymer concentrations.

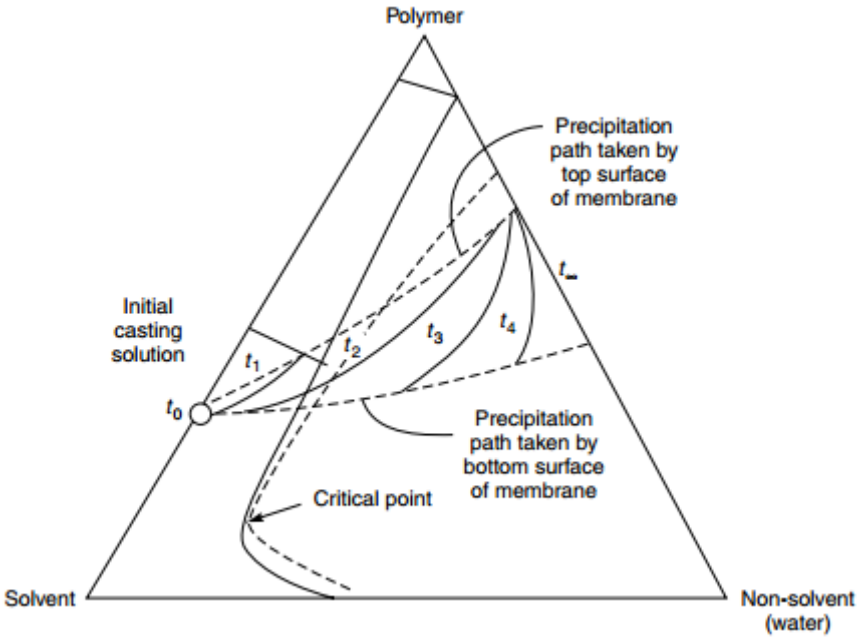

Figure 6: Precipitation pathways in binodal demixing [1].

Furthermore, getting into the finer details of the membrane formation mechanism, binodal demixing is the separation of the film into two phases, polymer rich and polymer lean. The

horizontal dashed lines in Figure 6 indicate the different separation pathways traveled by the phases during binodal demixing. The polymer rich phase (upper precipitation pathway) forms the dense top surface of the membrane, while the polymer lean phase (lower precipitation pathway) creates the more porous support structure of the membrane.

Membrane formation will be further discussed in more detail in the following two sections, the first one is the thermodynamics of the polymer system and the second is the mass transfer dynamics.

4.1.1. Thermodynamics of Polymer-Solvent-Nonsolvent Systems

Phase separation can be divided into three main categories depending on the parameters that induce demixing. The temperature at the polymer interface can be changed therefore resulting in demixing (temperature based). Phase separation can be induced as a result of a chemical reaction (reaction based). Lastly, the most widely used method, diffusion into the polymer solution (diffusion based) [31]. The membrane produced and its inherent properties are determined by the mechanism of demixing.

The membranes used for this study were all produced based upon diffusion induced phase separation, otherwise commonly referred to as non-solvent induced phase separation (NIPS). By contacting the polymer solution to a vapor or liquid, in this case liquid, diffusion based mass transport will result in local polymer concentration changes within the film thereby inducing demixing.

A three-step process is required for the phase inversion process. Firstly, there is gelation at the membrane non-solvent interface, resulting in the creation of a polymer dense layer. This is followed by the nucleation and growth of the pores because of the solvent outward flux and the non-solvent inward flux, these actions result in the membrane pore structure.

Lastly, there is another gelation process, which results in the bottom skin layer of the film. This again is the formation of a dense layer against the membrane substrate.

Depending on the substrate, however the mechanism will be different for gelation will be different. Since with the TFC membranes used in this study are cast on top of a wetted PET, a more open structure is created [18]. This is due to the excess solvent and the polymer essentially trying to integrate the non-woven into the matrix. Due to the openness of the non-woven void space is created which in effect results in a more open and porous membrane support layer being formed.

Phase inversion has been well described by the Flory-Huggins model for ternary systems [32-35]. The model takes into consideration both the entropy and the combinatorial factors of the polymer systems. The advantage of the model is its simplicity and wide applicability. One of the drawbacks is there are no excess volume considerations; instead a mixing approximation is used.

$$\frac{\Delta G_m}{RT} = n_1 \ln \varphi_1 + n_2 \ln \varphi_2 + n_3 \ln \varphi_3 + g_{12}(u_2) n_1 \varphi_2 + \chi_{13} n_1 \varphi_3 + \chi_{23} n_2 \varphi_3$$

The above equation is the extended Flory-Huggins theory as described by Mulder [32] and can be used to describe the formation of the dense top layer during phase inversion. Here the subscripts are; 1-nonsolvent, 2-solvent, 3-polymer. Where χ_{13} and χ_{23} are the nonsolvent-polymer and solvent-polymer interactions parameters, respectively. The ternary precipitation curves for PES/Solvent/Water can be seen below in Figure 7. As depicted PES is soluble in many aprotic solvents and is extremely tolerant to liquid-liquid demixing at a variety of conditions.

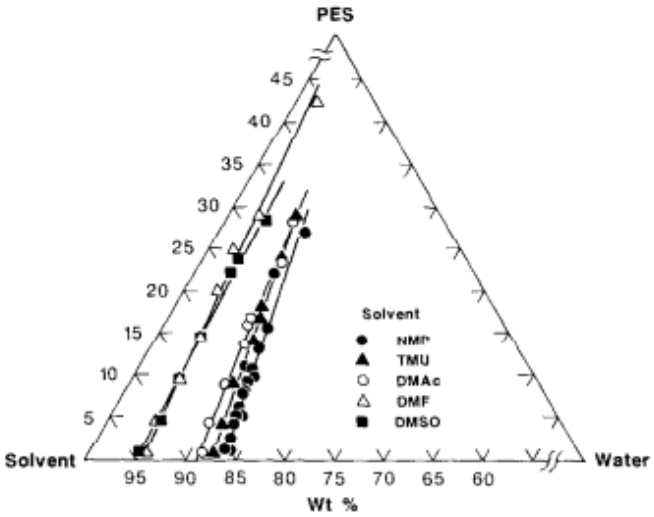

Figure 7: Ternary phase diagram of PES with various solvents (NMP, TMU, DMAc, DMF and DMSO) and water as the nonsolvent [36].

Increase in interaction between solvent and nonsolvent results in dense top layer. Decreased interaction between solvent and nonsolvent will render a more open porous top layer.

Additionally, the presence of a second solvent or nonsolvent into the polymer system has also been studied [31, 37]. The effects are dependent on the interaction parameters. The addition of a second solvent could either increase or decrease the overall interaction between the solvents and nonsolvent. The same thing could be said for the addition of a second nonsolvent. More generally, the properties of the quaternary system would lie in between the properties of the two separate ternary systems.

4.1.2. Mass Transfer Dynamics in Casting Solutions

Cohen, Tanny, and Prager provided the first mathematical model describing wet-cast phase inversion [38]. The model has some significant assumptions that were later modified by other investigators, for example, steady state diffusion, and the composition of the coagulation bath at the film interface is always that of the original bath. The underlying error in this assumption is that outward flux of the solvent is constant therefore a uniform pore

structure would be found throughout the entirety of the membrane as a result of either instantaneous or delayed demixing This poses a problem because distinctly different pore structures are created by instantaneous and delayed demixing.

The steady state diffusion assumption was considered inappropriate by some investigators [34, 35, 39]. Yilmaz and McHugh further expanded the model to pseudobinary diffusion formalism, assuming no polymer flux within the casting solution, along with negligible bath dynamics and constant partial molar volumes [35]. Experimental observations by Cabasso [40] showed that bath dynamics play a significant role in membrane formation due to the outward flux of the solvent and the inward flow of the nonsolvent. More recently, significant improvements to the model were made by Tsay and McHugh [41] to include interfacial composition changes with time. The primary assumption here is constant molar volumes; therefore, mass transfer can only occur by diffusion in both the film and the bath. The constant molar volume argument is that this assumption is inherent in the Flory-Huggins theory, as previously described for the phase inversion process. [42].

Depending on the polymer system, there are two different types of demixing as mentioned earlier, instantaneous and delayed. Instantaneous demixing results in asymmetric membranes with a dense top layer and large teardrop shaped macrovoids, whereas delayed demixing will result in more symmetric membranes with more sponge-like characteristics in the pore structure. The instantaneous demixing creates steep concentration gradients due to the relatively fast fluxes of the solvent and nonsolvent into and out of the polymer matrix, respectively; these fluxes dictate the nuclei growth within the film [43]. Because of this steep concentration gradient, it can be assumed that the mass transfer dynamics can be described as one-dimensional. If the process is delayed, or not instantaneous, then it will be a much more complex three-dimensional model [31].

On the other hand, symmetric structures are created from the delayed demixing because of more uniform nuclei growth. Delayed demixing does not lead to immediate instability compositions therefore more time is required to overcome the initial flux resistance.

Overall, final morphology depends on the interplay between solvent-nonsolvent inter-diffusion and polymer vitrification. Defining vitrification here are the process in which the casting solution solidifies crossing the glassy region in the phase diagram [44]. Looking specifically at macrovoid formation, this is a result of greater inward nonsolvent flux than outward solvent flux. McKelvey et al. describes this as nonsolvent diffusion front being faster than the vitrification front and creates conditions that allows for rapid demixing conditions and therefore sustaining the necessary driving force to create extended macrovoids [44]. Macrovoids nucleate from just below the free surface, so their growth can be suppressed if the vitrification front moves faster than the nonsolvent diffusion front; this will result in a macrovoid free sponge layer with denser surface layer [45].

In general there is no definitive theory on macrovoid formation, Smolder[45], gives a very thorough review of current theories and principles for macrovoid formation including a thorough analysis of instantaneous versus delayed liquid-liquid demixing of the polymer solution. It is generally accepted that inhomogeneities in the skin layer promote macrovoid formation through nucleation and growth in a polymer lean phase [44, 45].

4.2. Governing Equations for Membrane Processes

Characterization and modeling of flow through a membrane is very complex. The overall flux equation can be seen below**,** in which flux (J_w) is the negative product of the chemical potential gradient ($d\mu_i/dx$) multiplied by a proportionality constant (L_i). There are two distinct models used to describe the mechanism of transport through a membrane, the solution-diffusion and pore-flow models. [1, 46]

$$J_i = -L_i \frac{d\mu_i}{dx}$$

4.3. Solution-diffusion Model

The solution diffusion model describes flow as the dissolution of permeants into the membrane material and then diffusion through the membrane down a concentration gradient [1]. Separation is achieved between different permeants as a result of differences in the amount of materials that dissolves in the membrane and the rate that the material diffuses through the membrane [46].

$$\frac{d\mu_i}{dx} = \frac{dc_i}{dx}$$

The mode of transportation through the membrane active layer is diffusion and characterized by the solution diffusion model [46] as the mechanism of transport across the layer is governed by a concentration gradient, as shown in the equation above and depicted in Figure 8.

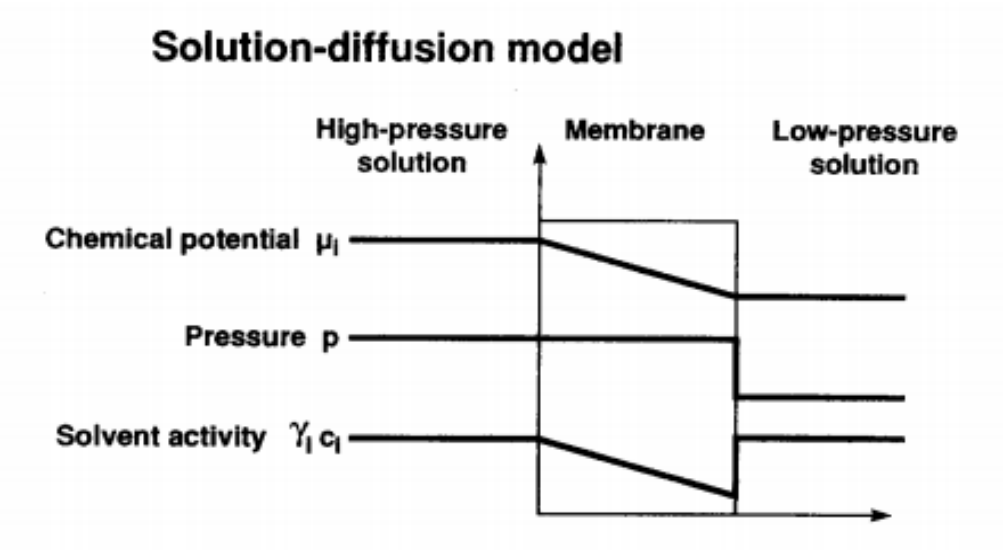

Figure 8: Membrane transport profile according to the solution-diffusion model. Adapted from [46]

Flow from the high-pressure side permeates through membrane active layer into the low-pressure side and the rejection of solutes results in the chemical potential gradient. The

solution-diffusion model is a good description for the transport mechanism through dialysis, reverse osmosis, gas separation and pervaporation membranes [46].

4.4. Pore-flow Model

The pore-flow model is much simpler than the solution-diffusion; it describes permeant transport through tiny pores due to pressure driven convective flow. The primary separation mechanism for this model is size exclusion. Particular permeants are permitted to pass through the membrane while others are prohibited because of being larger than the pore [1].

$$\frac{d\mu_i}{dx} = \frac{dp}{dx}$$

This type of flow can best describe the flow through the support layer, i.e. porous media where the primary driving force is convective flow.

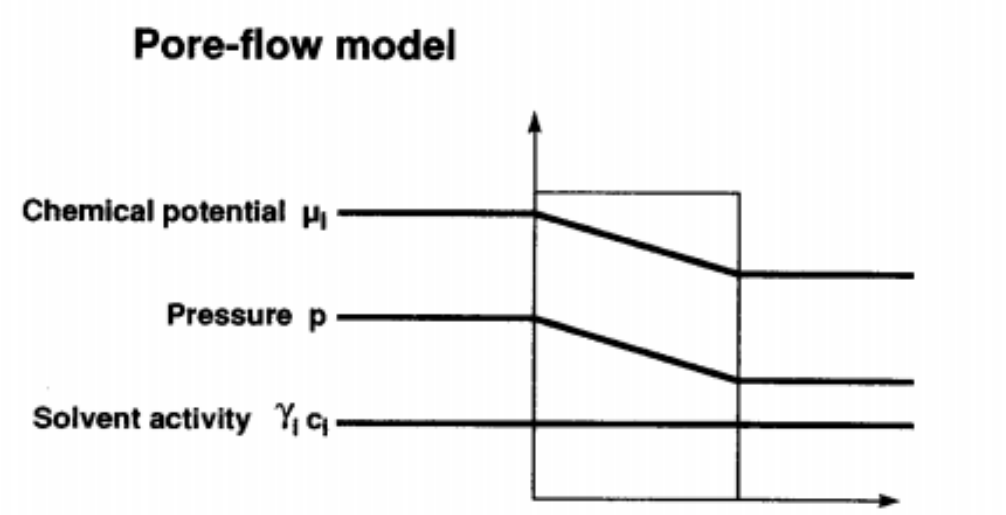

Figure 9: Membrane transport profile of the pore-flow model. [46]

The above figure shows the pore-flow model in which the chemical potential gradient can be seen as a pressure drop through the membrane support layer, this is due to the fact that the solute rejection has already occurred at the active layer. Membranes exhibiting the pore-flow mechanism are those, which rejection of divalent ions and organic solutes is good but

minimal rejection for monovalent ions [46]. Typical processes include particle filtration, micro filtration, ultra filtration, and loose nanofiltration.

4.5. Membrane Characterization and Performance Equations

There are several equations which are used for evaluating membrane properties and performance. These equations include, but are not limited to osmotic flux, solute flux, solute rejection, and concentration polarization (both internal and external).

The standard flux equation for membrane-based processes is below in Equation 1 where flux (Jw) is defined in a similar fashion as above; A is pure water permeability coefficient, and the driving force is the difference between the osmotic and the hydraulic pressures.

$$J_w = A(\Delta\pi - \Delta P) \qquad \text{Equation 1}$$

The salt or solute flux (Js) is defined similarly to the water flux in Equation 2, the product of the salt permeability coefficient (B) and the concentration difference between the feed and permeate solutions (ΔC). The observed salt rejection (R) described by Equation 3 is the difference between the concentration of permeate (C_P) and feed (C_F) solutions.

$$J_S = B\Delta C \qquad \text{Equation 2}$$

$$R(\%) = (1 - \frac{C_P}{C_F}) * 100 \qquad \text{Equation 3}$$

Concentration polarization (CP) is a significant problem in osmotic based membrane separation and has been reported extensively [1,5,10-16, 18-22]. Its presence negatively influences permeate flux by increasing osmotic pressure at the membrane active layer. There are two types of concentration polarization, internal (ICP) and external (ECP) [13]. ECP affects all types of membrane-based processes with the build-up of solute on the membrane active layer. This increases the necessary hydraulic pressure to overcome the osmotic pressure. ICP effects are seen in EO processes, this is the build-up of solutes within the

membrane support layer that result in the decrease of the overall osmotic pressure gradient [10].

The Figure 10 below represents the osmotic profiles of PRO mode (B) and FO mode (C). Profile A is representative of osmotic flow through a dense layer. Let it be known, that in the above figure, subscripts F represents the feed solution, while D represents draw solution, also subscripts b and m, are bulk phase and membrane interface, respectively. Overall, it can be seen that there is a loss of driving force in each of these profiles which results in an effective driving. This effective driving force is the result of solute build-up at the interfaces both inside and outside of the membrane.

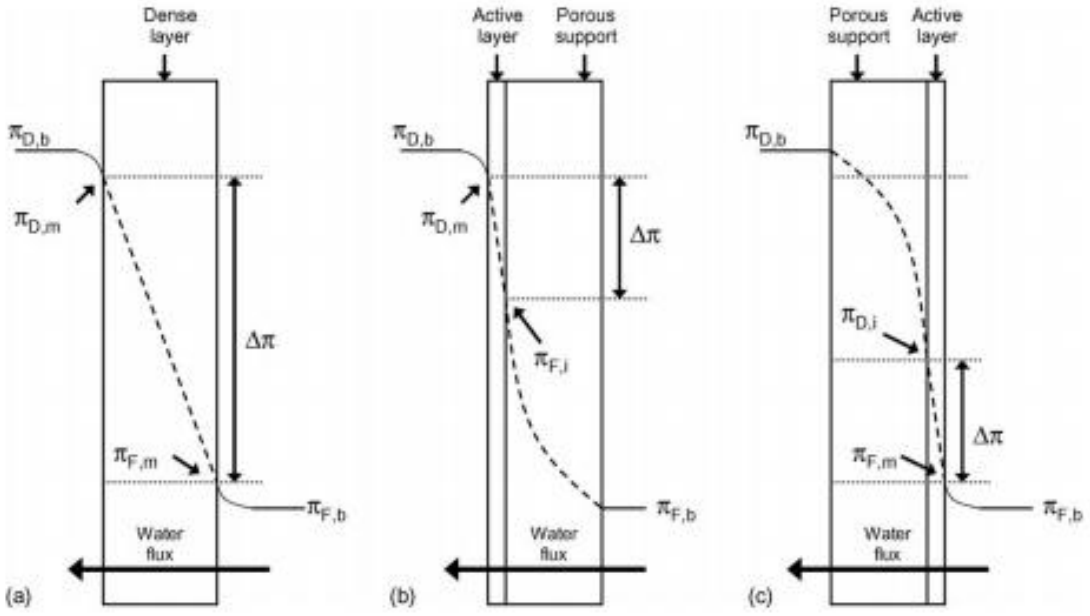

Figure 10: Osmotic pressure profiles in osmotic flux (A), PRO-Mode with concentrative ICP (B), and FO-Mode with dilutive ICP (C). [10]

External concentrative CP, as shown in profiles A and C, occurs at the active layer, where separation occurs, and is the result of convective water flow dragging solute from the bulk solution to the active layer surface resulting in greater resistance [10]. Dilutive external CP, as illustrated in profiles A and B, can be seen at the active-layer interface with the permeate solution (π_D). The dilution effect is seen as a result of convective flow taking draw

solute away from the membrane interface, ultimately reducing the effective driving force [10, 12, 14].

Lastly, internal concentration polarization, the more severe of the two, can be seen in profiles B and C above. Dilutive internal CP, as shown in the FO mode profile C, results from solvent permeating into the support layer and is diluted with the permeate solution coming through the membrane. Concentrative internal CP, occurs in PRO mode as seen in profile B, is when the bulk feed solution enters into the open pore structure of the support and since it cannot permeate the membrane active layer, it builds up at the interface, resulting in an increased concentration in the support layer [10, 12, 14].

Describing concentration polarization is done by correlating the effective concentration differences between the draw and feed or permeate and feed solutions to the observed differences as depicted in Equation 4. This is then related to the CP modulus, the exponential of water flux divided by the mass transfer coefficient (k) as seen in Equation 5.

$$\frac{\Delta C_{effective}}{\Delta C_{observed}} = \frac{C_{membrane} - C_{permeate}}{C_{bulk} - C_{permeate}} = e^{(\frac{Jw}{k})} \qquad \text{Equation 4}$$

$$k = \frac{Sh \cdot D_{AB}}{d_h} \qquad \text{Equation 5}$$

The mass transfer coefficient is defined as the product of the Sherwood number (Sh) and the solute diffusivity (D_{AB}) divided by the hydraulic diameter (d_h) of the channel. Furthermore, depending on the type of CP, the CP modulus with either be positive or negative. For FO processes, the CP modulus will lower the effective osmotic pressure of the draw solution by having a negative sign, whereas on the feed side of the membrane, it will increase the osmotic pressure at the membrane interface with having a positive sign on the exponential. These two effects as discussed previously will result in a lower overall osmotic pressure difference. In all cases, the CP modulus contributes negatively to overall osmotic performance. McCutcheon et al. determined that the negative CP contributions increase with

Equation 6

increasing flux, therefore creating a situation where flux is self-limiting and increases in bulk osmotic pressure provide diminished increases in flux [10].

$$K = \left(\frac{1}{J_w}\right) \ln \frac{B + A\pi_{D,b}}{B + J_w + A\pi_{F,m}}$$

$$S = KD = \frac{t_s \tau}{\varepsilon} \qquad \text{Equation 7}$$

Moreover, two other factors for gauging membrane performance are the solute resistivity for diffusion within the porous support layer (K) [13] and the structural parameter (S). Described in Equation 6, K is a function of water flux, osmotic driving force and permeability, both water and solute. The structural parameter, described by Equation 7, is the product of solute diffusivity and K. Minimizing the overall structural parameter is key for obtaining optimum membrane performance.

5. Materials and Methods

5.1. Polymers

Solvay Advanced Polymers (Alpharetta, GA) supplied PES and SPES. The PES was post sulfonated using concentrated sulfuric acid under various conditions to create several degrees of sulfonation.

Data for polymers is provided in Table 1. The PES is commercial grade Radel-A (Mw 66,000 g/mol) from Solvay Advanced Polymers.

Polymer	Comment	Free Acid Titration (µeq/g)	Mw (g/mol)	Water flux (g/min) at 45 psig	Permeability (LMH/Bar)
PES	Base		66,481	<1	6.11
SPES-05	Increasing	27	66,315	3	18.3
SPES-07	Sulfonation	38	66,207	28	171
SPES-09		30	66,271		
SPES-03		384	52,739**	>100	611

Table 1: Data for polymers used in study, including free acid titration, molecular weight (Mw), and initial water flux from films cast at 300 µm at 45 psi.

5.2. Chemicals

Let it be known that all chemicals were used as received unless noted.

5.2.1. Solvents

N-methyl-2-pyrrolidinone (NMP, anhydrous 99.5%) and Acetone (ACS Grade) were obtained from Fisher Scientific.

5.2.2. Monomers

Two monomers were used for the interfacial polymerization process, a diamine and an acid chloride. The diamine monomer m-phenylenediamine (MPD, >99%) and the acid chloride monomer 1,3,5-benzenetricarbonyltrichloride (TMC, 98%) were purchased from

Sigma-Aldrich. For the remainder of the thesis, the monomers will be referred to as MPD and TMC respectively.

5.2.3. Isopar-G

Proprietary non-polar organic solvent which the TMC is dispersed (Gallade Chemical). Isopar-G will from now on be referred to as Isopar.

5.3. Deionized (DI) Water

DI water was used for all fabrication, washing, and testing purposes. The water was obtained from a Milli-Q ultrapure water purification system (Millipore, Billerica, MA).

5.4. Polyester (PET) non-woven

Poly(ethylene terephthalate) (PET) non-woven substrate (PET, Sanko 16-1) was acquired from the Sanko Junyaku Co., Ltd (Japan) and was used as a membrane support for the TFC membranes.

Additionally, another other PET (Freudenberg, Weinheim, Germany) non-woven was used for permeability testing.

5.5. Commercial asymmetric Cellulose Triacetate (CTA) FO membranes

Commercial asymmetric cellulose triacetate (HTI-CTA) FO membranes (Hydration Technology Innovations Inc., Albany, OR) were acquired for performance comparison.

5.6. Polymer Solution Preparation

Polymer solutions were prepared on a weight percent basis. Fisher band glass mixing bottles (250 mL) and PTFE coated stir bars were used for all solutions. Appropriate amounts of polymer and solvent were weighed using an analytical balance and placed into bottles. Note, bottles and stir bars were first properly cleaned with acetone, dried in a drying oven

prior to use. First solvent was placed into bottles and set upon a stir-plate at a rotational velocity of 250 rpm. Then the polymer was added in order to ensure optimum mixing. Solutions were allowed to stir at room temperature for at least 8 hours, once polymer was fully dissolved, they were left at room temperature for some time until air bubbles were not longer seen, normally two hours.

Furthermore, since SPES-03 is the most sulfonated polymer, it was decided that blending it with the pure PES could reveal the possibility of an optimum sulfonation level. The blended polymer solutions were made in the same manner as the pure polymer solutions, as described previously. Table 2 provides the details of the various blends used in the study.

Polymer Loading (wt. %)	**12%**	**16%**	**20%**
Blend Ratio	**1:1** **1:2** **1:4** **1:8**	**1:1** **1:2** **1:4** **1:8**	**1:1** **1:2** **1:4** **1:8**

Table 2: Experimental matrix for SPES-03: PES blends.

5.7. Membrane Preparation

The membranes presented in this work have been made using the nonsolvent induced phase separation mechanism as described earlier. A thin film of polymer solution is cast onto a glass plate using a casting knife. The film is then immersed into a nonsolvent bath (water) and the liquid-liquid demixing begins and ultimately produces a polymeric membrane.

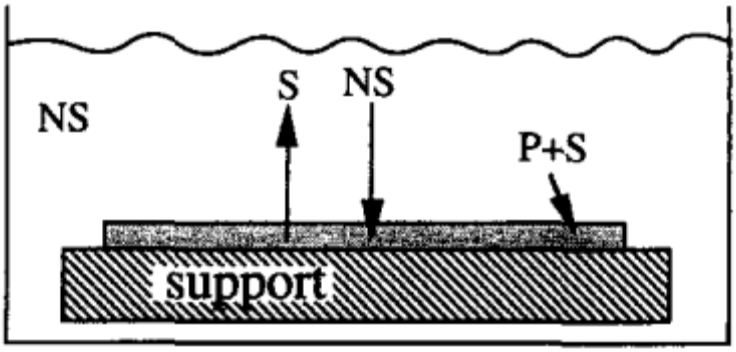

Figure 11: Diagram of immersion precipitation process. [43]

The diagram depicts the casted film (P+S) on top of a support, with the arrows indicating the relative direction of the solvent and nonsolvent out of and into the film, respectively.

Described below are the two methods for which the asymmetric membrane support layers and the TFC membranes were produced.

5.7.1. Asymmetric

5.7.1.1. Casting Protocol

All films used for initial testing were made in the same manner using the following protocol. Using a 10" x 10" (25.4 x 25.4 cm) clean glass plate, pour an amount about 1-1.5" (2.5-3.7 cm) thick and 7-8" (17.8-20.3 cm) wide at the top of the glass plate. Using the custom-made casting knife draw the solution down to the bottom of the plate. Then immerse into 1L of DI water for approximately 10 minutes. During the first minutes the film should float to the surface of the water, this is indicative of the phase inversion process being complete. Once the 10 minutes have been reached, carefully lift the film from the water bath, rinse it several times with DI water from a squirt-bottle, and then place it into another DI water bath. After several minutes the membranes should be washed again using DI water then cut into appropriate pieces for storage in DI water in the refrigerator (5°C) until testing.

5.7.2. Thin Film Composite

The thin film composite membrane procedure is a two step process. First asymmetric membrane support layers are made using the phase inversion process, very similar to the aforementioned process. Then the membranes are interfacially polymerized with TMC and MPD for the addition of the ultra-thin polyamide layer.

5.7.2.1. Casting Protocol

The membrane supports are made by first taping a piece of PET non-woven is taped to the glass plate. Then the PET is wetted out using 3-4 mL of NMP and a rubber roller. Once the non-woven is uniformly wet and the excess NMP has been removed the polymer solution is poured out in a similar manner as in the asymmetric protocol. The casting knife is then used to draw the solution down therefore making a thin film. The glass plate with the film is then placed into a 1L DI water bath for 10 minutes. Afterwards the glass plate with the film-casted non-woven is to be removed, rinsed with DI water several times then placed into a secondary DI water bath. From here the non-woven can be removed from the glass plate, rinsed with DI water again, then cut to appropriate size and placed into a container with DI water and into the refrigerator (5°C) until further use.

5.7.2.2. Interfacial Polymerization Process

Interfacial polymerization as mentioned above it the formation of an ultra-thin selective layer at the dense surface of the asymmetric membrane. This is done by forcing two monomers (MPD and TMC) to polymerize at the membrane interface. The MPD is dissolved into water and the TMC into Isopar . Due to the polarity differences between the two phases the monomers react with one another at the surface to produce a polyamide.

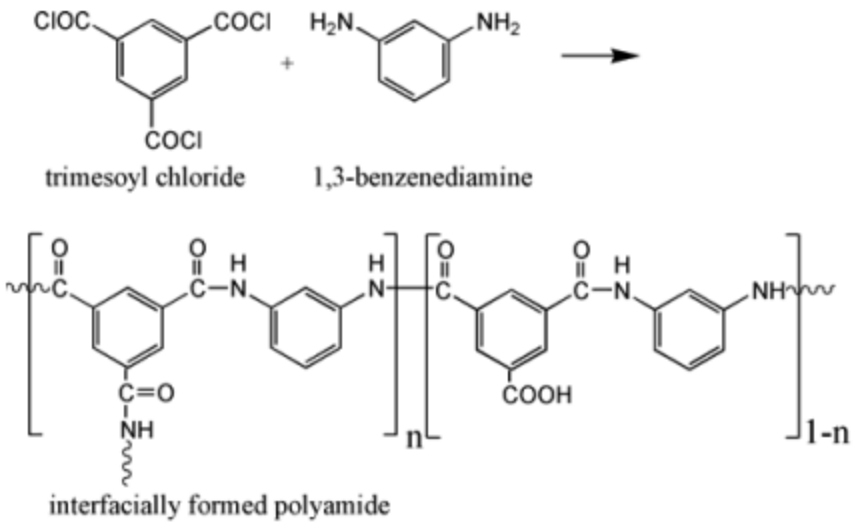

Figure 12: Polyamide formation by reaction between TMC and MPD [47].

The detail of the process are as follows:

First tape the non-woven (PET) to glass plate, then apply 3-4 mL of NMP to surface using pipette and spread it evenly using rubber roller. It is best to remove any air visible air pockets as they will create defects during the casting process. Next pour out the same amount of polymer solution as would be normally used for casting an asymmetric membrane as described above. Draw down the solution to produce a thin film and then place the glass plate with the PET and the film into 1L of DI water for 10 minutes. After the elapsed time, remove the glass plate with the PET and the film, rinse with a DI water bottle, then place into a secondary water bath for several minutes. At this time, remove the PET from the glass plate; remove any excess PET with scissors or razor blade.

Next the asymmetric membranes are dipped into first an MPD-DI water solution (6.8% wt. MPD) for 2 minutes, then excess solution is removed using a rubber roller. Following this the membrane is dipped into the TMC-Isopar solution (0.15% wt. TMC) for 1 minute, removed and allowed to evaporate for a pre-determined amount of time (1-4 minutes). The samples are placed into an oven at a preset temperature (80-90°C) for a specific amount of

time (5-7 minutes). Samples were then rinsed in two DI water baths (5 minutes per bath) in order to remove any residual MPD and TMC.

5.8. Membrane Testing

Several methods for testing both the asymmetric and thin film composite membranes were utilized for characterization. The asymmetric membranes were characterized first in order to determine which polymers were going to be further tested for the interfacial polymerization process. Asymmetric membranes were studied thermally, chemically, and physically. The thin film composite membranes were tested in reverse osmosis and forward osmosis systems to determine water permeability, water flux and solute rejection performances.

5.8.1. Asymmetric Membranes

5.8.1.1. Thermogravimetric Analysis (TGA)

A TA Instruments (New Castle, DE) TGA Q-500 was used for thermogravimetric analysis. Samples sizes of 15-18 mg of polymer precursor were tested. The samples were placed into the pans and the predetermined method was loaded into the TA instruments software. The method initialized the chamber to 30 °C, and then ramped at a rate of 10 °C/min to 900 °C. All mass changes were automatically logged using the TA Instruments software. Analysis was completed using TA Instruments Universal Analysis software.

5.8.1.2. Differential Scanning Calorimetry (DSC)

Differential scanning Calorimetry was completed using a DSC Q-2000 from TA Instruments. Samples were massed out using analytical balance; approximately 5-7 mg of polymer precursor was used. Polymer precursor was placed into aluminum hermetic pans with lids, obtained from TA Instruments. The DSC is a power consumption DSC in that it

requires a reference pan and records the power required to heat the sample to the same temperature as the reference.

TA Instruments Universal Analysis software was used for testing, data collection, and analysis. The testing method initially stabilizes the temperature of the chamber to 25°C, and then ramps at 10°C/min to 300°C. The conditions are held constant at 300°C for two minutes, and then sample is then ramped down to 25°C at 10 °C /min. The system is then ramped again at 10°C/min to 350°C. Analysis was competed using mid-point calculations on the second cycle. The second cycle was chosen in order to remove any thermal history of the polymer, therefore providing a truer glass transition temperature.

5.8.1.3. Dynamic Mechanical Analysis (DMA)

A Dynamic Mechanical Analyzer 2980 from TA Instruments was used for stress at break testing of the asymmetric films. Tests were run at 25 °C and a ramp rate of 0.5 N/min. Average sample size was 12 mm x 9 mm. Samples were removed from their container, surface dried with Kim-Wipes, measured and cut to size with a razor-blade. Data acquisition and analysis was completed using the Universal Analysis software from TA Instruments. Values presented below are the average of three tests.

5.8.1.4. Contact Angle

Contact angle goniometry is a method used for determining the wettability i.e. hydrophilicity of a surface. It is best described by the Young equation.

$$\gamma_{LV}\cos\theta = \gamma_{SV} - \gamma_{SL}$$

The Young equation uses surface tension and the angle with which the substance, in this case water contacts the surface in order to measure the contact angle and interfacial energy. In the above equation, the subscripts represent the interfacial energies of the

solid/vapor (SV), solid/liquid (SL) and liquid/vapor (LV) interfaces. Contact angle measurements were used for determining relative hydrophilicity.

Samples were prepared by casting polymer dope solutions at 50 um on to glass plates then placing them into a vacuum oven at 150 °C and -25 in. Hg for 15 hours. Contact angle was measured using DI water with a Cam 101 series contact angle goniometer (KSV Company Linthicum Heights, MD). The values calculated are the average of at least six tests with a droplet size of 6.0 ± 1 µL.

5.8.1.5. Scanning Electron Microscopy (SEM)

SEM was performed with a Phenom from FEI (Hillsboro, OR) to look at the surface and cross-sectional properties of the films. The surface images were prepared by cutting a piece of film and placing it upon the stage in the correct orientation. For the cross-sectional images, membranes were fractured in liquid nitrogen to retain the pore structure and then mounted to a stage using carbon tape. Samples were sputter coated with gold-palladium plasma at a current of 20 mA for approximately 150 seconds under a vacuum in an argon environment. Sputter coating was done in order to avoid charge accumulation upon the samples and ensure viewing in the SEM.

5.8.1.6. Permeability

Permeability testing was done using an Amicon 8050 cell from Millipore (Billerica, MA). The feed was DI water and tests were run using 15 (1.03), 30 (2.07), 45 (3.10) and 60 psi (4.14 bar) driving forces. Permeate was collected in a cup and weighed using a balance. The membrane samples were prepared using a 1 5/8" (4.12 cm) punch from McMaster-Carr (Robbinsville, NJ). At least three different membrane samples were tested. The Solvay steel was used for the data acquisition of the handmade PES and SPES membranes.

5.8.1.6.1. Mesh Effects

An investigation into the effects of the mesh support on membrane permeability was also completed. This was a result of during the early stages of asymmetric film characterization discrepancies were observed during permeability testing. Initial testing using the Control Nylon resulted in relatively high permeabilities. It was later determined that the water flux values provided in Table 1 by Solvay Advanced Polymers were done using a stainless steel mesh (Solvay Steel). The observed permeabilities using the Solvay Steel were significantly different from the Control Nylon. Since the pore openings of the two respective meshes are very similar to one another it was believed that the mesh material played a significant role in permeability. In order to verify that it was indeed the material and not an effect of the membrane defects a commercial membrane (STL-01 from 3M (Meriden, CT)) was used incorporated into testing.

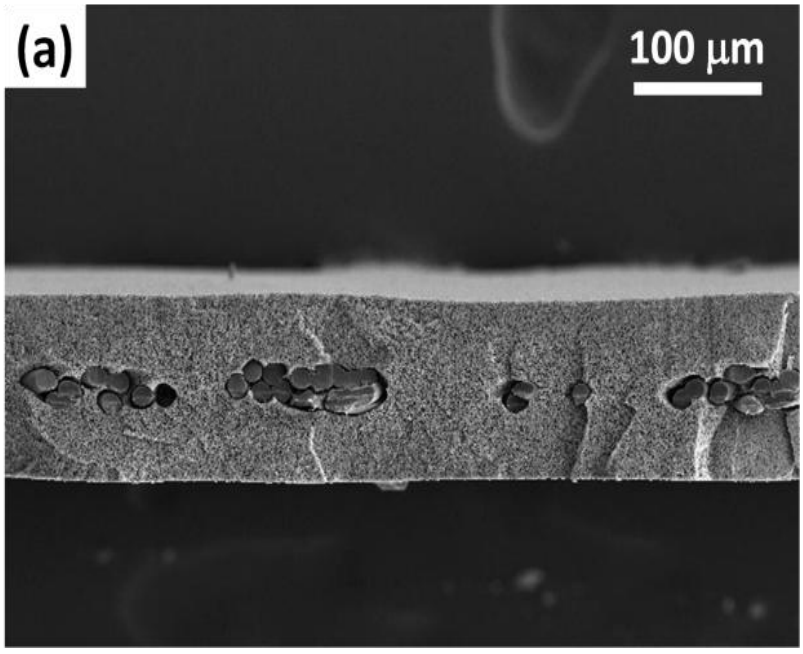

Figure 13: SEM cross-section of STL-01 membrane. Provided by 3M.

Support	Average Pore Size (um)	Thickness (um)	Porosity (%)	Surface Porosity (%)	Contact Angle (Degrees)
STL-01	**0.025**	**150**	**70**	**52.8**	**41.8**

Table 3: Properties of STL-01 membrane. Provided by 3M.

The STL-01 was an ideal membrane choice for the support layer testing because it is symmetric and has properties (porosity and pore size) as seen above in Table 3 very similar to those obtained from the Mercury Intrusion Porosimetry testing, as is described in more detail later on.

Support Mesh	Control Nylon	Sefar Nylon	Solvay Steel	Fine Steel Mesh	Non-Woven
Pore Opening (um)	**214**	**40**	**275**	**50**	**N/A**
Material	**Nylon**	**Nylon**	**Stainless Steel**	**Stainless Steel**	**PET**
Image	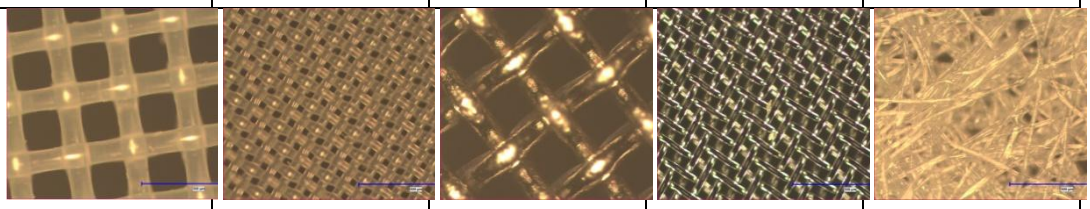				
Scale	**500 µm**				

Table 4: Properties of various support mesh used in permeability testing for STL-01 membrane.

As seen in Table 4 five separate meshes were used, two nylon, two stainless steel, and one PET non-woven. Furthermore, a scenario with no mesh acted as a control. Two nylon

and stainless steel meshes were chosen so that it could be determined if pore opening had an influence on membrane permeability.

5.8.1.7. Mercury Intrusion Porosimetry (MIP)

Mercury intrusion porosimetry (MIP) was used determine pore size distributions of the support layers. The technique involves the intrusion of a non-wetting liquid, in this case mercury, at high pressure into the membrane material. Through use of the Washburn equation, the pore size diameter (D) can be determined based upon the external pressure (P) and the surface tension of the penetrating liquid (mercury).

$$D = (-4\gamma \cdot \cos\theta)/P$$

It was assumed that the contact angle ($\cos\theta$) of mercury was constant at 140° and the surface tension (γ) was 480 dynes/cm [48, 49]. Advantages of MIP include the detection of both through and blind pores. Through pores are those which extend the length of the membrane, blind pores are those which do not extend the length of the material. One of the drawbacks of MIP is compression, due to the nature of the method, high pressures are used that could compress the material therefore creating biases.

Membranes are cast using a 50 µm casting rod using the same casting protocol as described earlier. The casted solutions are then removed from their secondary wash baths and placed on paper towel in the hood and allowed to dry for approximately 24 hours. The membrane density needed to be determined in order to prepare the samples for the Mercury Intrusion Porosimeter. A 1 5/8" (4.12 cm) punch from McMaster-Carr was used to obtain samples from the cast membrane sheets. Ten samples were stacked on top of one another, a micrometer was used to determine their thickness, they were then weighed using an analytical balance, and membrane densities were calculated. Once the samples prep was complete for

each membrane, the bulk porosities and pore size distributions were determined using an AutoPore IV by Micrometrics (Norcross, GA). A range of pressures from 0-60,000 psi (0-4137 bar) were used to obtain pore diameters in from 0.003-360 um. Triplicate tests were run for each membrane in order to accurately calculate an average and a standard deviation.

5.8.2. Thin Film Composite Membranes

Membrane active layers were fabricated by interfacial polymerization as described previously. This was done by polymerizing two monomers at the membrane interface in the presence of an organic and an aqueous phase. The MPD was dissolved into water (aqueous), and the TMC into Isopar-G (organic), by virtue of polarity differences the two solvents will not mix, therefore when they are exposed to one another the monomers are forced to react.

5.8.2.1. SEM

TFC membrane samples were imaged using a JEOL (Tokyo, Japan) JSM-6335F field emission scanning electron microscope (FESEM). Sample preparation was done by removing the PET layer from the cast film and then fractured using liquid nitrogen as described earlier. The samples were sputter coated using gold and palladium as described previously, to obtain better contrast and avoid charge accumulation. An accelerating voltage of 10 kV and a working distance of 7 mm and 10 mm for the cross-sectional and surface images, respectively.

5.8.2.2. Reverse Osmosis Testing

Testing was done primarily in accordance with [50]. Membranes were loaded into cells and equilibrated for at least 1 hour at 100 psi. Permeability was then determined from permeate flux at 50, 100, 150 and 200 psi (3.45, 6.90, 10.4, and 13.8 bar). Salt was then added to the system and permeate, salt permeability, and salt rejection were determined from flux at 225 psi (15.5 bar). A schematic of the test system is below in Figure 14.

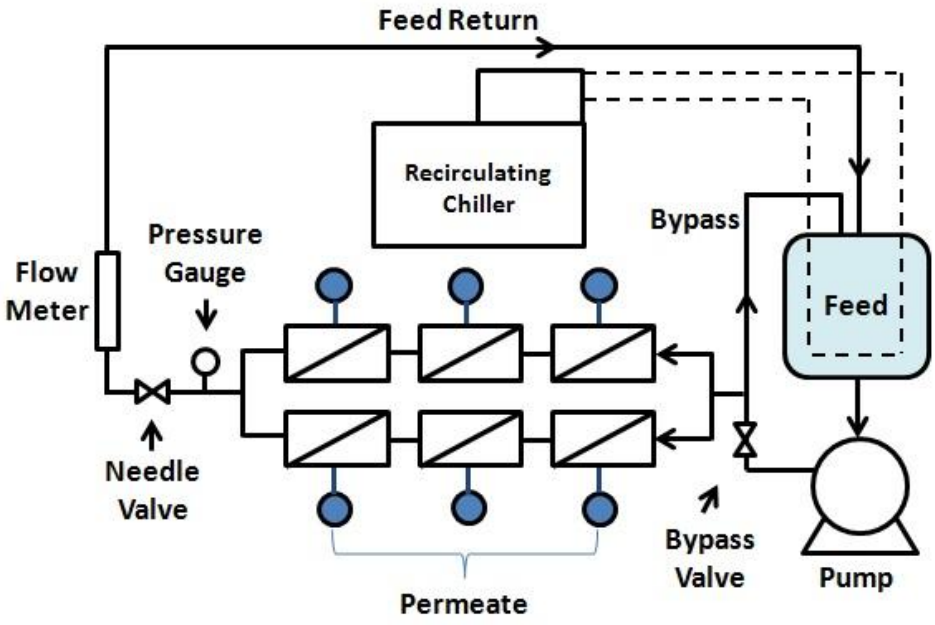

Figure 14: Diagram of six-celled Reverse Osmosis system.

System is composed of six RO cells that use a diaphragm pump to provide a flow rate of 1L/min (Re~1300) through the cells and a recirculating chiller to maintain a constant temperature of 20 °C.

5.8.2.3. Forward Osmosis Testing

Testing was completed on a custom-built counter-current osmosis cell as shown below in Figure 15. The system has been described previously in literature [20-22]. Osmotic flux was tested in FO mode (support layer against draw solution) using 0.05, 0.1, 0.5, 1.0, and 1.5M NaCl draw solutions. Salt flux and structural parameters were calculated from values at 1.5M NaCl. Separately sodium dodecyl sulfate (SDS) was added to a concentration of 1 mM into the draw solution to look at membrane wetting, this was done using a 1.5M NaCl draw solution. For all tests, the temperature was held constant at 20 °C and a flow rate of 1 L/min (Re~1300).

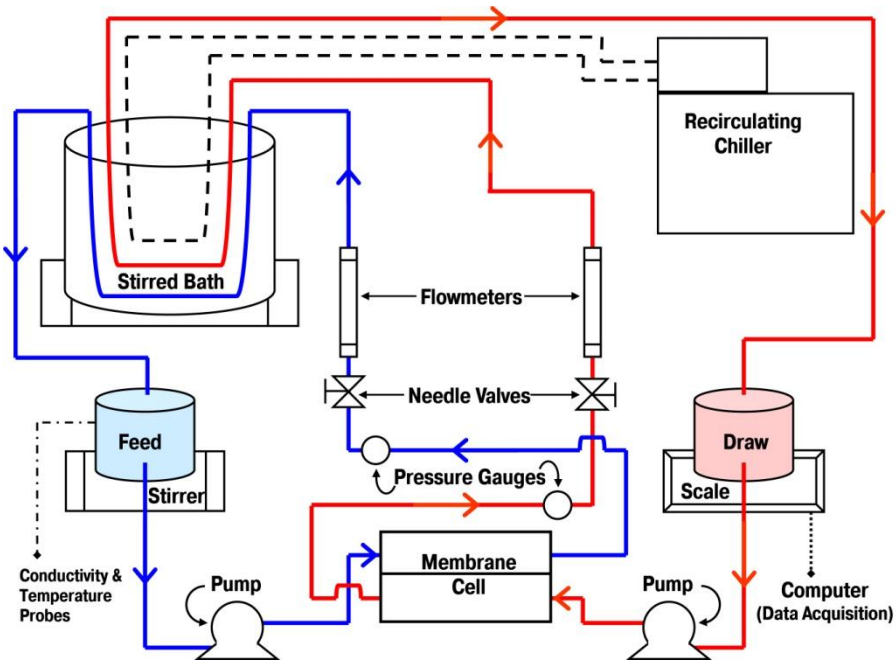

Figure 15: Schematic of forward osmosis test system.

6. Results

The results are split up into two sections, one for the asymmetric membranes and the other for the thin film composite membranes. For nomenclature clarification, all membranes will be designated by their polymer i.e. polyethersulfone supports will be referred to as PES membranes. Secondly, all thin film composite membranes will be known as TFC.

6.1. Asymmetric Membranes

Asymmetric membranes were fabricated and tested using the methods described previously in Section 5.71.1.

6.1.1. SEM 50 & 150um Cast Films

Polymer films were cast at both 50 and 150 µm onto glass plates. The resulting films as discussed were freeze fractured in liquid nitrogen, sputter-coated and viewed under an SEM. The images of the membranes can be seen below in Figures 16 & 17.

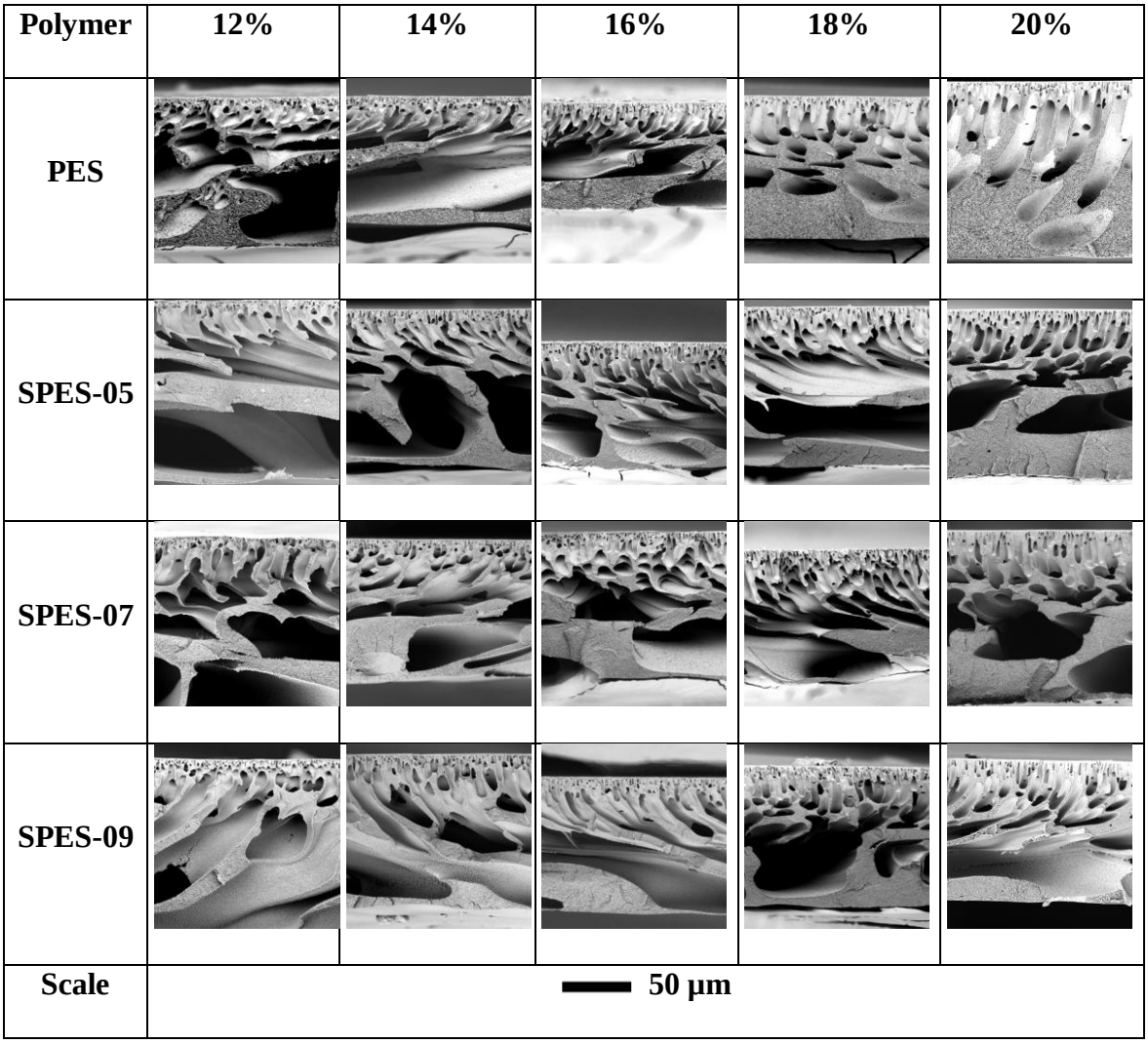

Figure 16: SEM **c**ross-sections of membranes cast at 150 µm onto glass plates. The left column denotes the polymer used and reading from left to right polymer loading (wt %) increases from 12%-20%. All polymers were dissolved in NMP.

As shown in the figures all polymers were cast at both 50 and 150 µm and with polymer loadings ranging from 12%-20% by weight. Overall looking for trends among the structures it is difficult to make any clear cut observations, but it can be seen that the thickness of the bottom layer or the membranes tends to increase as polymer loading increases (from left to right). This is most likely due to a shift in the binodal curve, which in effect changes the point that demixing occurs. Since there is more polymer at higher loading, the interaction parameters between the polymer, solvent and nonsolvent are not the same as

they are at lower concentrations, this results in the various pore structures. In general, instantaneous demixing is seen in every case from the large finger-like pores present.

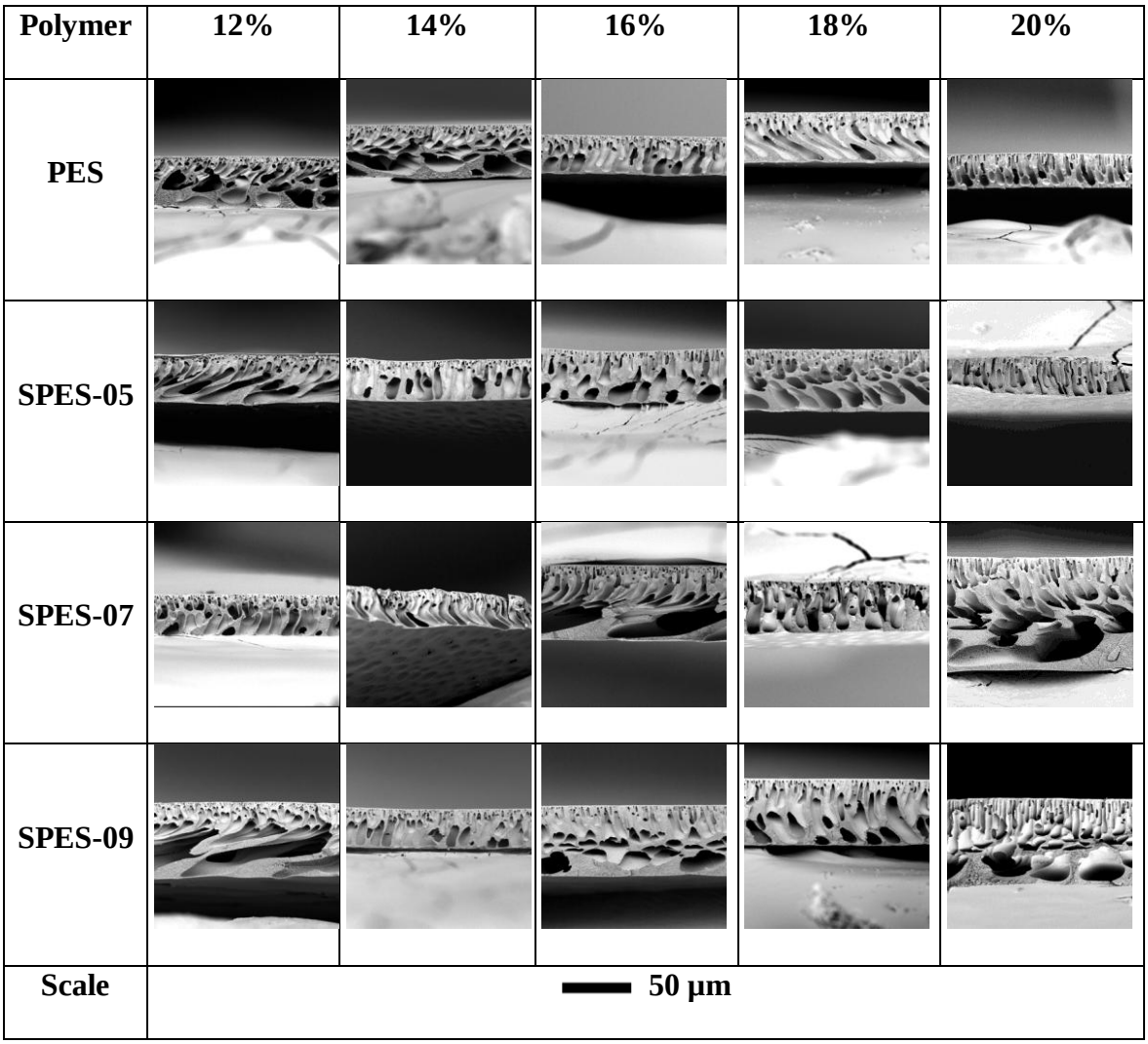

Figure 17: Cross-sections of membranes cast at 50 µm onto glass plates. The left column denotes the polymer used and reading from left to right polymer loading (wt %) increases from 12%-20%. All polymers were dissolved in NMP.

As mentioned previously, for an ideal membrane support, an open, porous, thin, non-tortuous (finger-like) pore structure is preferred. Based upon these properties the 14% polymer solutions films cast at 50 µm provide the ideal pore structures.

SPES-03 was also cast in the same method as the above polymers, however as can be seen below, resulting membranes are far different. Several trials were made for SPES-03 to see if a pore structure similar to those already presented could be seen. Two separate solvent

systems, as well as two coagulation bath compositions were tested. Two 20% SPES-03 solutions were made, one with pure NMP and another with 1:3 DMF:NMP ratio.

Coagulation Bath: H2O	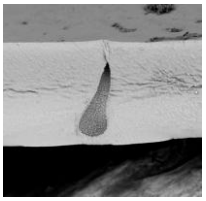	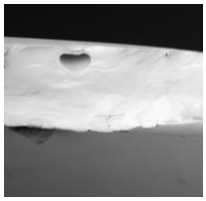	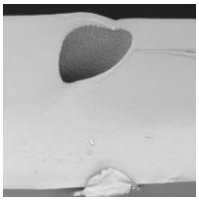
Solvent System:	**NMP**	**NMP**	**DMF:NMP (1:3)**
Coagulation Bath: 3% NMP in H2O	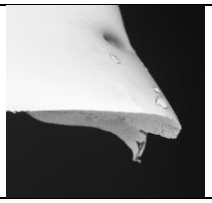	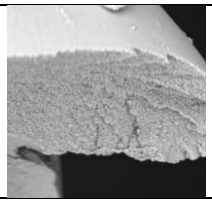	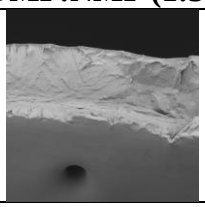
Scale Bar: ▬▬ 50 µm			

Figure 18: SEM cross-sections of 20% SPES-03 films cast at 150 µm with two different solvent systems and coagulation baths.

Additionally, two coagulations baths were looked at, pure DI water and 3% NMP in DI water. It was believed that changing the dynamics of the phase inversion would elucidate a different pore structure; however, that was also not seen as depicted in Figure 18. From the SEM images it is apparent that no macrovoids are present in the pure SPES-03 films, this is very indicative that non-instantaneous (delayed) demixing occurred as the mechanism for precipitation. The change in liquid-liquid demixing was likely a result of interaction parameters, specifically χ_{13}, brought on by the sulfonation. The increase in sulfonation results in a decrease of solvent-polymer affinity. The effects of this, according to McKelvey et al. [44], are delayed demixing, resulting in the vitrification front being faster than the nonsolvent diffusion front.

Of the blends tested, the 1:2, 1:4 and 1:8 proved to meet the handling ability criteria. The 1:2 and 1:4 ratios however could only be handled enough for SEM preparation when cast at 150 µm and at polymer loading greater than 12%. The 1:8 blend, as expected provided the

best characteristics of all of the blends. As show in Figure 19 the pore structure created from the 50 µm cast films is very desirable and at all of the polymer loadings.

SPES-03:PES Ratio	Scale Bar	12%	16%	20%
1:2	100 µm	X	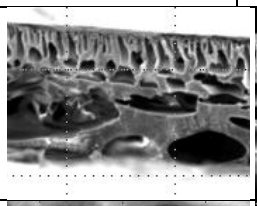	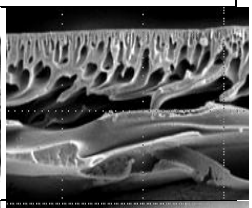
1:4	100 µm	X	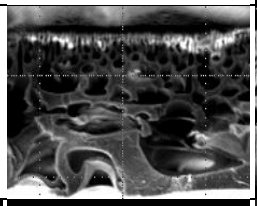	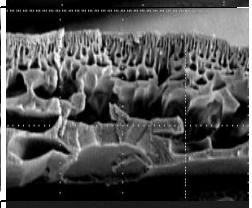
1:8	10 µm	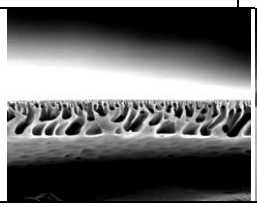	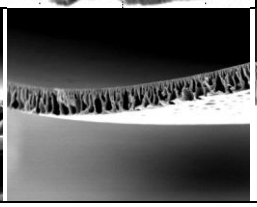	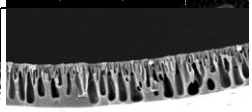

Figure 19: SEM cross-sections of SPES-03: PES blended solutions.

Furthermore, qualitatively it was noticed that the demixing time decreased as the amount of PES in the polymer solutions increased. In other words, the liquid-liquid demixing went from delayed to instantaneous. This is further evidence that the interaction parameter χ_{13} is being influenced by the degree of sulfonation.

6.1.2. TGA

Thermogravimetric analysis (TGA) was used to determine the thermal stability of the polymers and to try to verify the degree of sulfonation of the polymers. It has previously been noted by Guan [51] that near 400 °C the sulfonic acid groups will degrade corresponding to a

weight loss. The percent loss in weight is indicative of the percent sulfonation. The data is presented below in Figure 20.

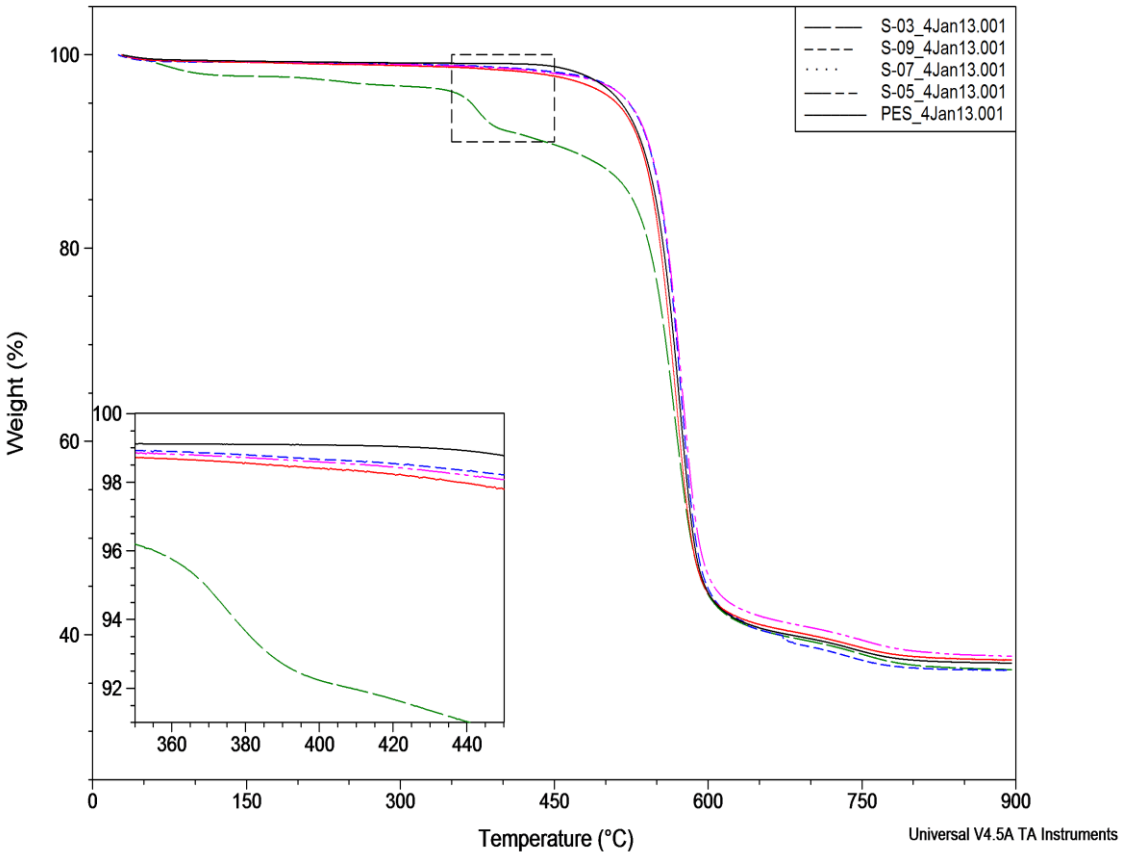

Figure 20: Thermogravimetric Analysis curves for polymer precursor.

From the data it can be seen that the polymer degrades in order of SPES-03>SPES-07>SPES-05>SPES-09>PES near 400 °C as indicated by the inset in the plot window. Due to the data being so closely coupled, it is inherent that low degrees of sulfonation were for all polymers except SPES-03 as expected. It was not possible to calculate the exact percent sulfonation from the TGA data.

It should be noted that the sulfonation did not greatly decrease the decomposition temperature as has previously been shown [52].

6.1.3. DSC

Digital Scanning Calorimetry (DSC) was used to determine the glass transition temperature (Tg) of the PES and SPES polymers used in the study. Glass transition temperatures are an indication of how the polymer chains are affected by the sulfonation process. All samples as mentioned before are pure polymer precursor. It is expected, that as sulfonation increases, the glass transition temperature will increase due to more limited mobility of the polymer chains. Therefore more energy will be required for the chains to begin sliding past one another, i.e. reach a glassy state. Another way of interpreting the glass transition temperature is by a spike in the heat capacity. This is beginning of the polymer moving to the upper temperature range of the solid phase. Let it be known that the glass transition is not a transition from solid to liquid, but rather a transition from glassy to rubbery. Also gives a reasonable indication of the upper temperature limit with which the polymer can be used for particular applications. In this instance, for membrane formation and ultimately water purification and treatment, since application temperatures will not be above 200 °C, the glass transition is not an issue.

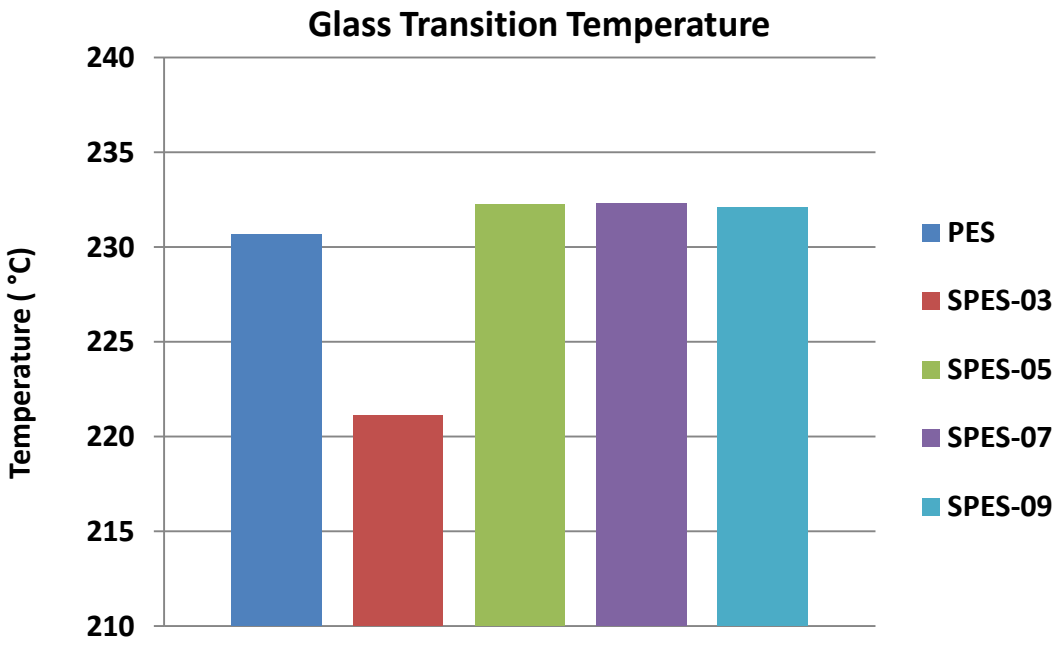

Figure 21: Digital scanning calorimetry results for polymer precursor. All values calculated by midpoint analysis with TA instruments software.

From the data it can be seen that the PES has a Tg just over 230 °C, then SPES-05, SPES-07, and SPES-09 have slightly greater Tg's, closer to 234 °C, indicative of the polymer chain being more restricted. Just as previously seen in the TGA data, since the data is so closely coupled it is known that the polymers were sulfonated to relatively similar degrees. The SPES-03 has a much lower Tg as a result of the much greater degree of sulfonation. The polymer has undergone a significant loss of molecular weight due to the sulfonation reaction. The reaction resulted in chain scissions and therefore smaller polymer chains. Since the chains are smaller they can move around more easily at a lower temperature, in this case the Tg is just above 220 °C.

6.1.4. DMA

Dynamic mechanical analysis (DMA) was performed on asymmetric membranes in order to determine the amount of stress the films could handle before they broke. The break point is the moment the membranes tears into two pieces.

From the data in Figure 22 it can be seen that the films made from the sulfonated polymers can handle close to 60% of the stress that the unmodified PES films can. This is an indication that the films are weaker and could fail more easily during testing especially when at higher operating pressures. As is expected, the more sulfonated the polymer the lower the stress at break.

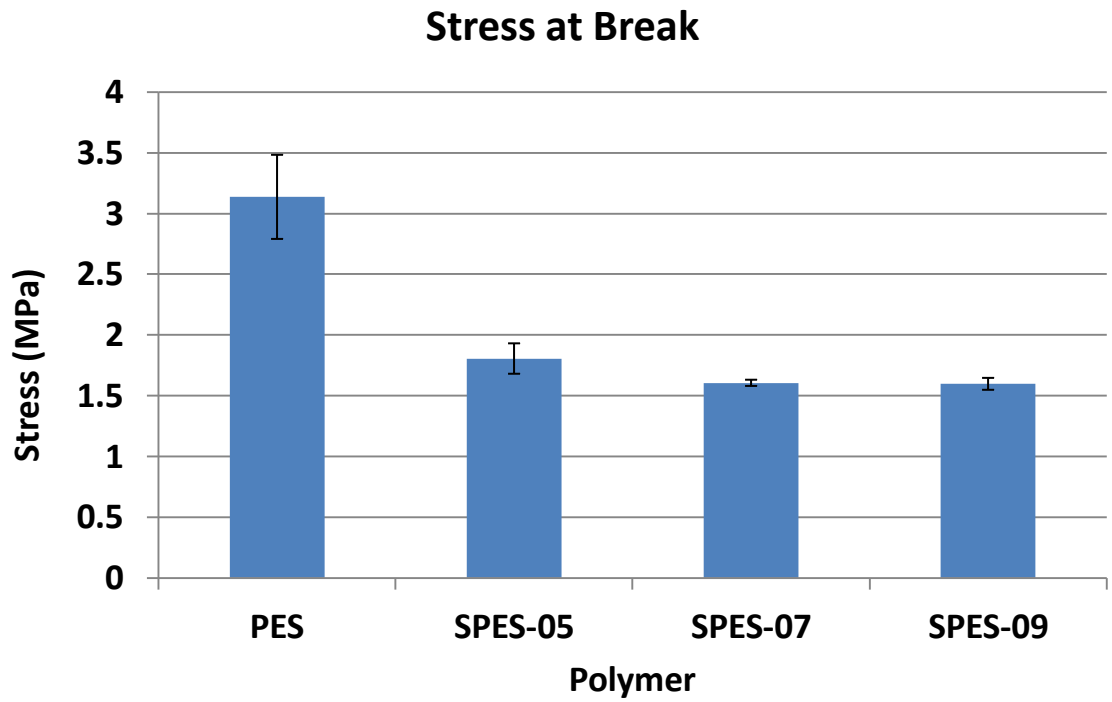

Figure 22: Dynamic mechanical analysis data for 20% polymer loading in NMP cast at 150µm.

The results are for the support layers. In RO testing, the TFC membranes have a polyamide layer attached to them that will result in some addition strength. Additionally, the stress here was applied laterally, in the lengthwise direction. In an osmosis cell the force is applied normal to the active layer, so the results here are not entirely telling of the membrane strength, but a good indication that post-sulfonation results in films that have a lower stress at break.

6.1.5. Contact Angle

There looks to be a clear trend in contact angle data, as sulfonation increases the contact angle of the polymer films decreases. The contact angles decrease in the order with which they were mentioned previously (Table 1), except for SPES-07. It was expected that SPES-07 would have a value between SPES-05 and SPES-09 but it appears to be greater. Overall, it can be seen that the modified polymers are more hydrophilic, as seen by the lower contact angles than the unmodified PES in Figure 23.

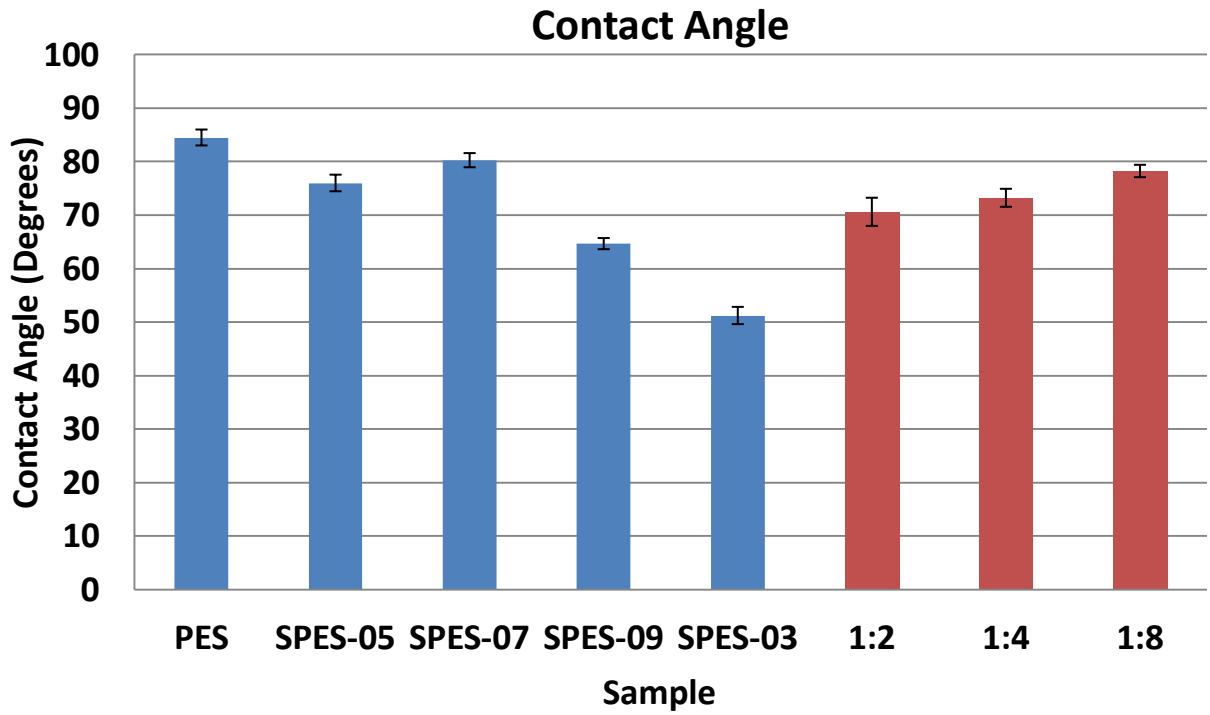

Figure 23: Contact angle data for polymer films cast at 50 µm. Films were cast on to glass plates, put into a vacuum oven at 150 °C at -25 in. Hg for approximately 15 hours.

With respect to the polymer blends, as anticipated, blending resulted in an increase in hydrophilicity. As seen in Figure 21 with increasing amount of PES in the blends, the contact angle increases. Furthermore, the values obtained for the blends are in the range of the pure PES and SPES-03 contact angles, indicating that blending is a possible option for increasing the hydrophilicity of the films.

6.1.6. Permeability Testing

Pure water permeability obtained from the asymmetric samples tested in the Millipore Amicon cell can be seen in Figure 24. The graph indicates that the modified polymers exhibit greater water permeabilities in comparison to the PES.

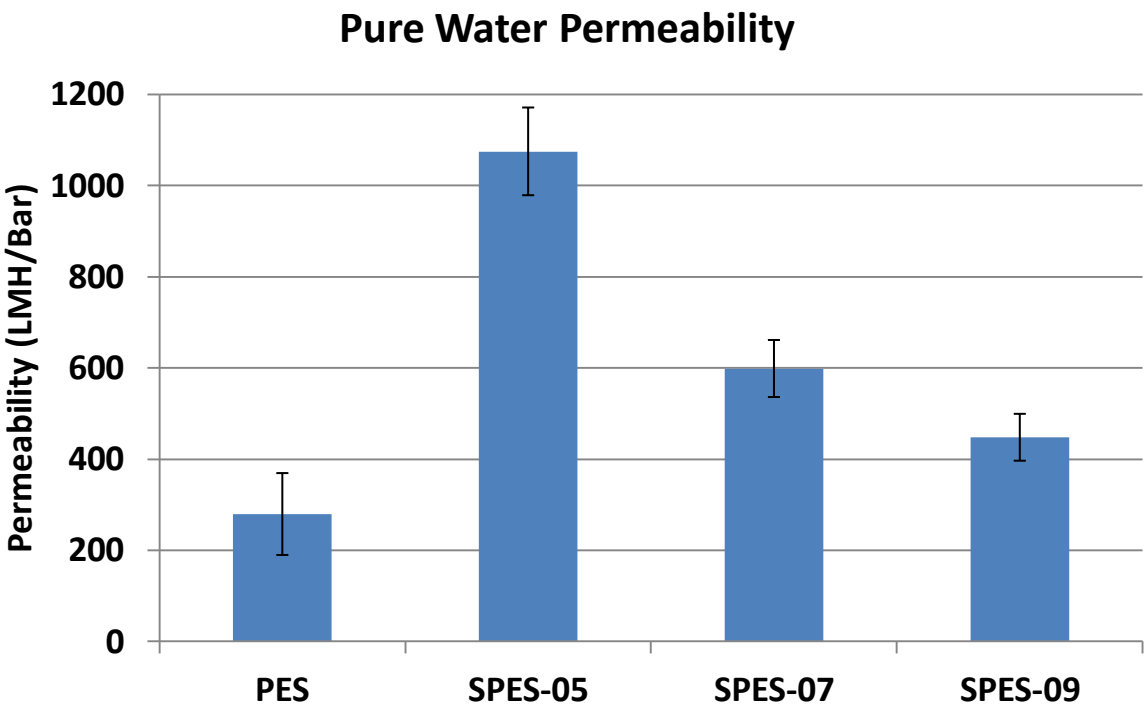

Figure 24: Pure water permeability for 20% polymer loading in NMP cast at 150 µm. Values are the average of at least three tests. Solvay steel was used at the support in the Amicon cell.

This again is indicative that the polymers have been modified to make them more hydrophilic and therefore less resistant to water flow. One thing of interest is that as the degree of sulfonation increases, the permeability decreases, contrary to what was expected. SPES-03 was not tested because the asymmetric films were too weak to handle, they became defective when placed into the Amicon cell.

As is further discussed in the next section from the MIP results, it can be seen that as sulfonation increases, the bulk porosity contribution from the smaller pores increases. This is indicative that there are more smaller pores in the asymmetric films of the sulfonated

polymers. The pure water permeability does not necessarily reflect this because high enough pressures were not used to force water into the smallest pores of the membrane, entry pressure can be calculated from the Washburn Equation as mentioned previously. Again, the trend of the permeability data above suggests that sulfonation does not increase permeability, but this may not be entirely true due to pore size differences.

Furthermore, the pure water permeability of the blended membranes was also determined, using the same methodology as with the pure polymer support layers.

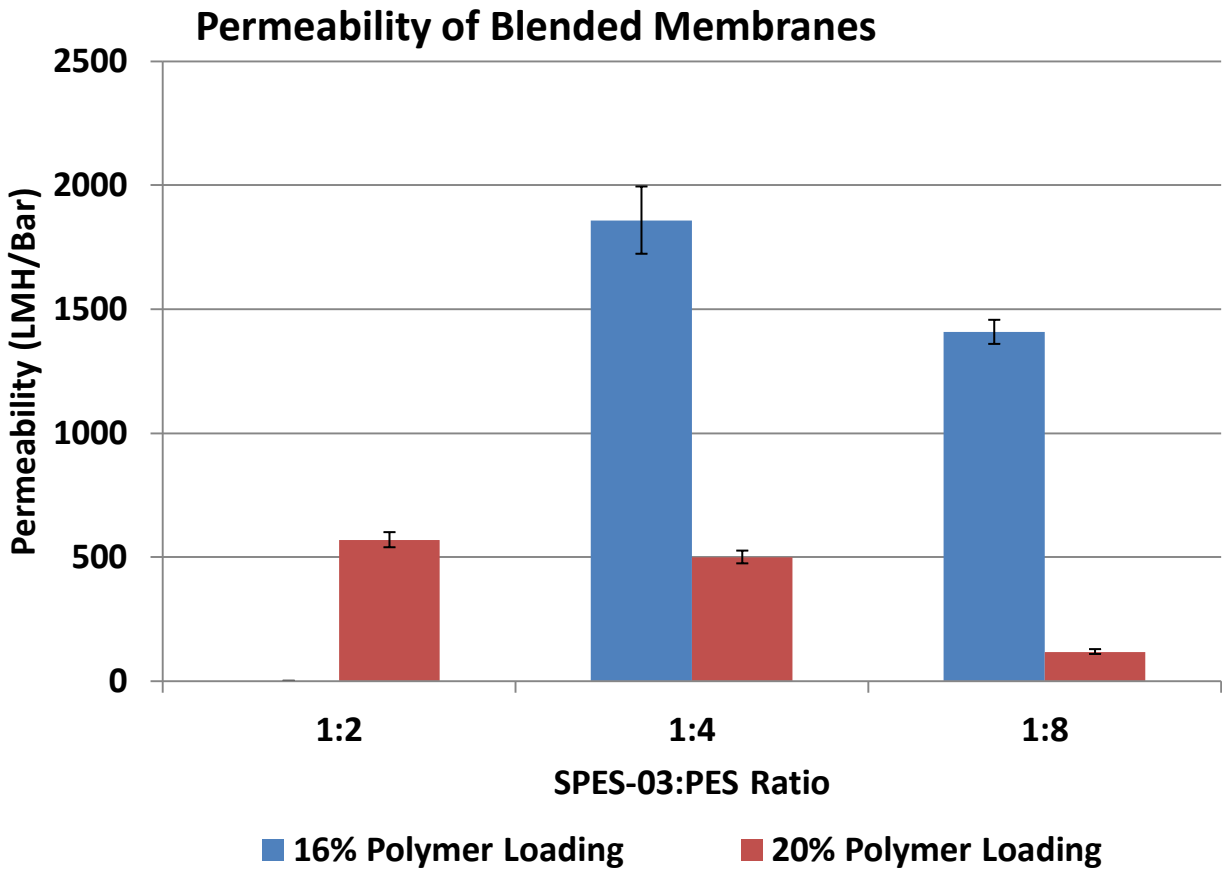

Figure 25: Permeability of SPES-03:PES blended membranes cast at 50 µm at 16% and 20% polymer loading in NMP.

The blended membranes exhibit water permeabilities similar to those of the pure polymer support layers. From Figure 25 it is seen that two different polymer loadings were tested, in order to verify findings. Permeability decreases as the amount of PES increases in

polymer blend, 1:4 > 1:8. This is further seen in the 20% polymer films in which 1:2 has the greatest permeability, followed by 1:4 and the 1:8 blends.

Comparing the blended permeability values to those of the pure polymer membranes, the blended values are very similar to the values shown in Figure 24. The highest permeability value from the 1:2 blended membranes at 20% polymer loading is around 600 LMH/Bar, which is about the same as the permeability of the SPES-07 membrane. Looking at the 16% polymer loadings of the blended membranes the permeabilities are much higher than the SPES-05 membrane, indicating the blending is facilitating greater water transport as a result of the increased hydrophilicity.

6.1.6.1. Mesh Spacer Effects

Six different scenarios were tested to deduce the effects of support mesh on membrane permeability. From Figure 26 it is evident that both material and pore opening play a role in membrane permeability.

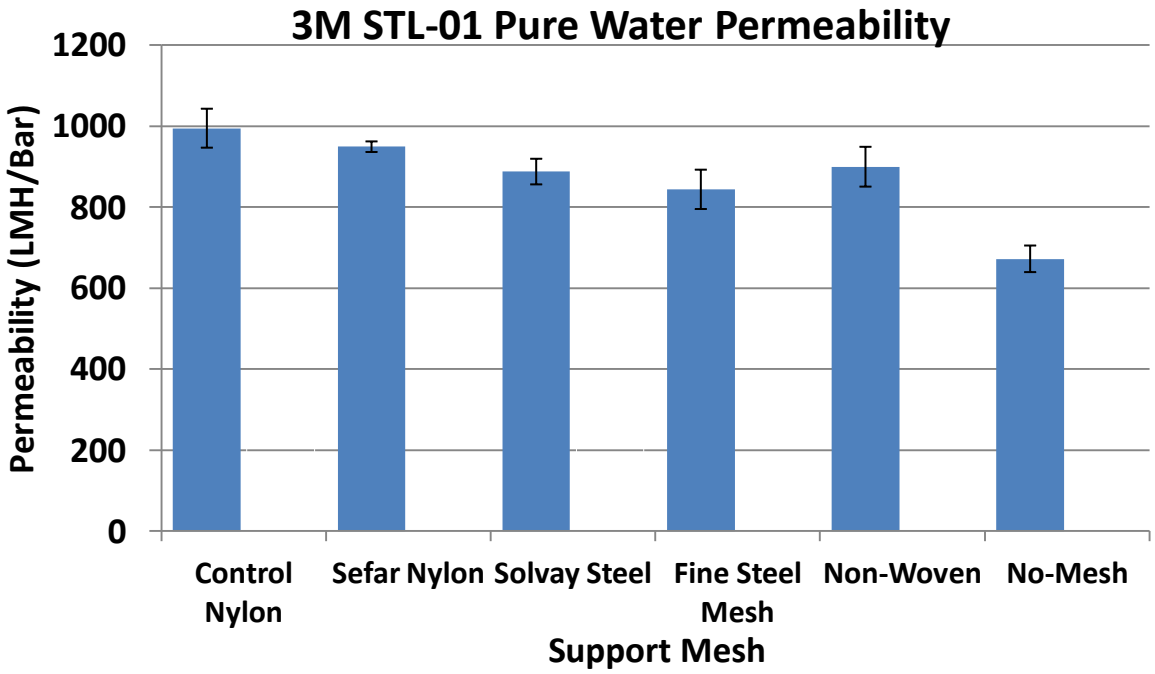

Figure 26: Effects of various support mesh on the permeability of commercial STL-01 membrane.

The highest permeability was produced with the Control Nylon, the nylon with the largest pores, while the smallest permeability was seen with no mesh. It is believed that the pore opening has a minor role in the overall scheme of permeability in comparison to the material properties that have a much greater impact on membrane permeability. Kim et al. noted a similar trend with permeability effects and membrane support [53]. It was believed that pore stretching was the primary mechanism for the increased permeability. Along the same lines, based upon the rigid structure of the bottom of the Amicon cell it was thought that pore stretching also occurred in our tests. The bottom of the cell allows for the mesh support to fit to the contours of the cell and when the pressure is applied to the membrane an increased surface area is created due to the shape.

Looking at the different support meshes there are several variables that can be tested; opening size, material, and rigidity. First taking mesh opening into account, from both the nylon and the stainless steel permeability values it is seen that the larger opening meshes generate larger permeabilities. Additionally, both nylon meshes have higher permeabilities than the two steel meshes. The Control Nylon has the highest permeability, followed by the Sefar Nylon, the Non-Woven, then the stainless steel meshes and lastly no-mesh. Overall, it was found that more hydrophilic materials, nylon and PET provided larger permeabilities. As for mesh rigidity, because the stainless steel meshes are stronger and more rigid than the nylon and the non-woven they do not promote the increased surface area and pore stretching that are seen with the other meshes. This ultimately, is a positive effect because the experimental permeability is most likely to be more representative of the actual permeability. Lastly, looking to the control scenario of no-mesh, the lowest permeability was generated here. This is likely a result of the membrane fitting to the bottom of the Amicon cell but the shape of the cell inhibits water flow so it consequently increases resistance to flux. After discussing each of these one by one it is apparent that material hydrophilicity is the most

important factor for permeability, however, the most representative is the Solvay steel because the large pore opening limits resistance and its rigidity forces the membrane to maintain its properties.

6.1.7. Mercury Intrusion Porosimetry (MIP)

The MIP data is separated into two figures in order to illustrate two different topics. The first as seen in Figure 27 is the effect of polymer loading on membrane pore size distribution.

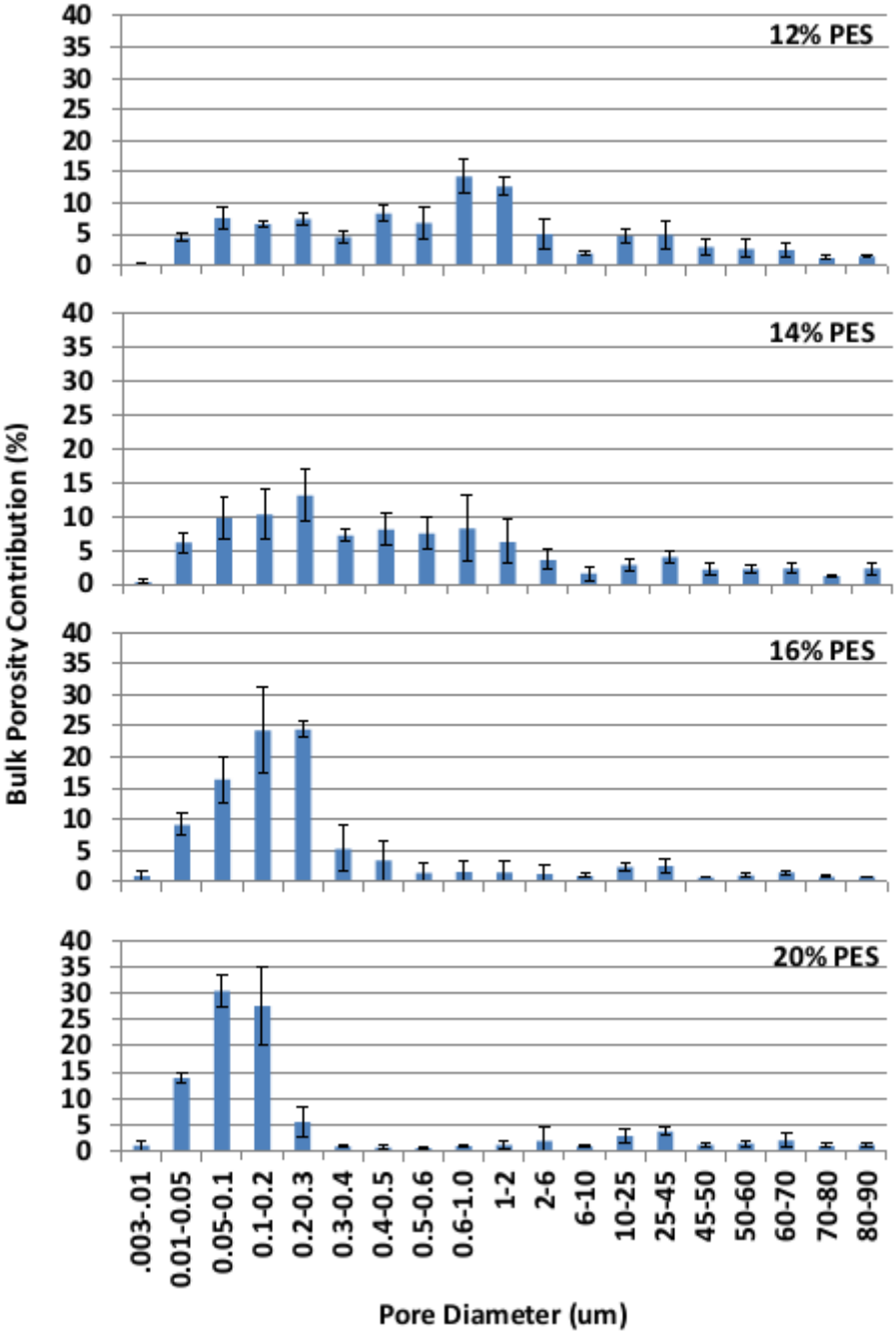

Figure 27: MIP data, effects of polymer loading on the bulk porosity contribution of specific pore diameters.

The figure above clearly illustrates that as polymer loading increases, moving from top (12%) to bottom (20%) the bulk porosity contribution of the smaller pores increases, as indicated by the bars shifting to the left side of the graph.

The second subject investigated was the effects of sulfonation on membrane pore size, and this can be seen below in Figure 28.

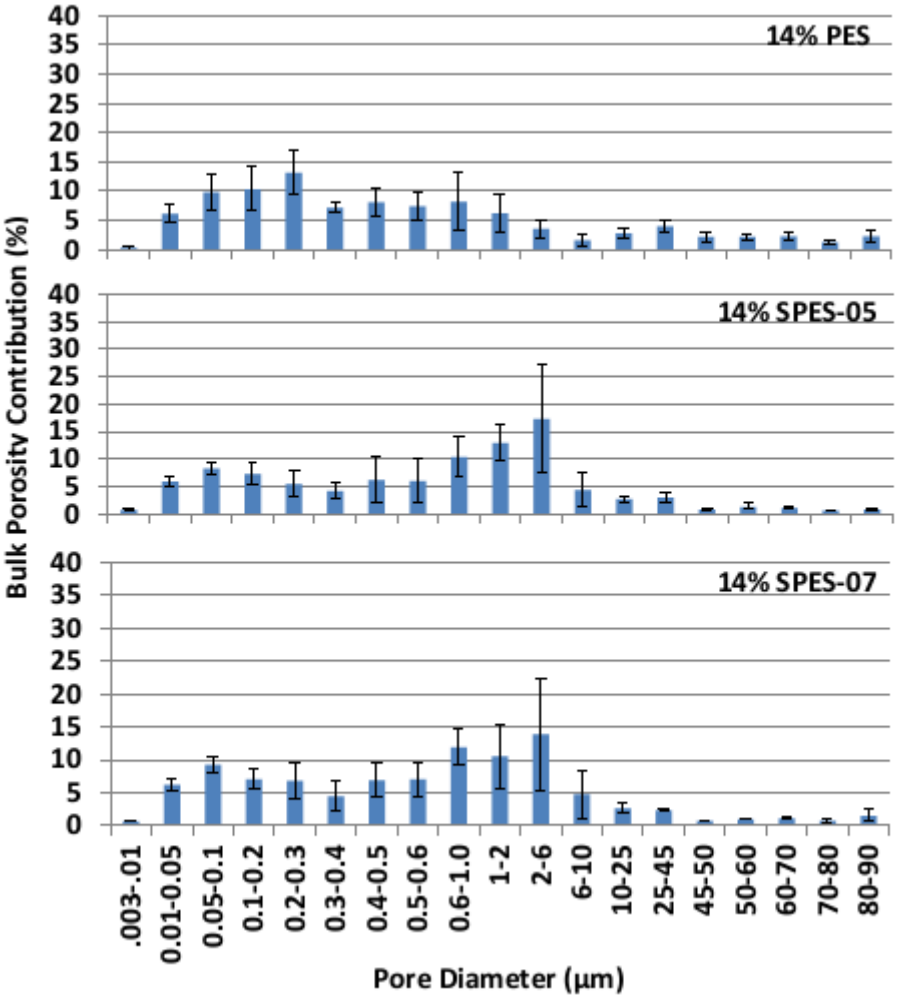

Figure 28: MIP data, effects of sulfonation on 14% polymer loading in NMP.

Sulfonation, as expected, increases the amount of pores in the membrane, as demonstrated in Figure 28. One thing to note, as alluded to earlier, as the degree of sulfonation increases, more smaller pores are present in the membranes. This is contrary to what would be expected because of the use of more hydrophilic polymers. However, according to the thermodynamics and mass transfer dynamics it follows theory. Due to the greater affinity for the polymer to the nonsolvent (water) in the coagulation bath, more

delayed demixing is seen in comparison to the pure PES. Due to the more delayed demixing a more spongy structure is being formed. This was not seen in the SEM cross-sections because the pore sizes are sub-micron, but proves to be the logical explanation based upon literature.

Bulk porosity data as shown in Figure 29 indicates membrane porosity is generally independent of polymer loading and sulfonation. Porosity contributions from smaller pores increase as sulfonation increases and polymer loading. Due to the relatively low differences in degrees of sulfonation, large bulk porosity changes are not seen, if they play a role.

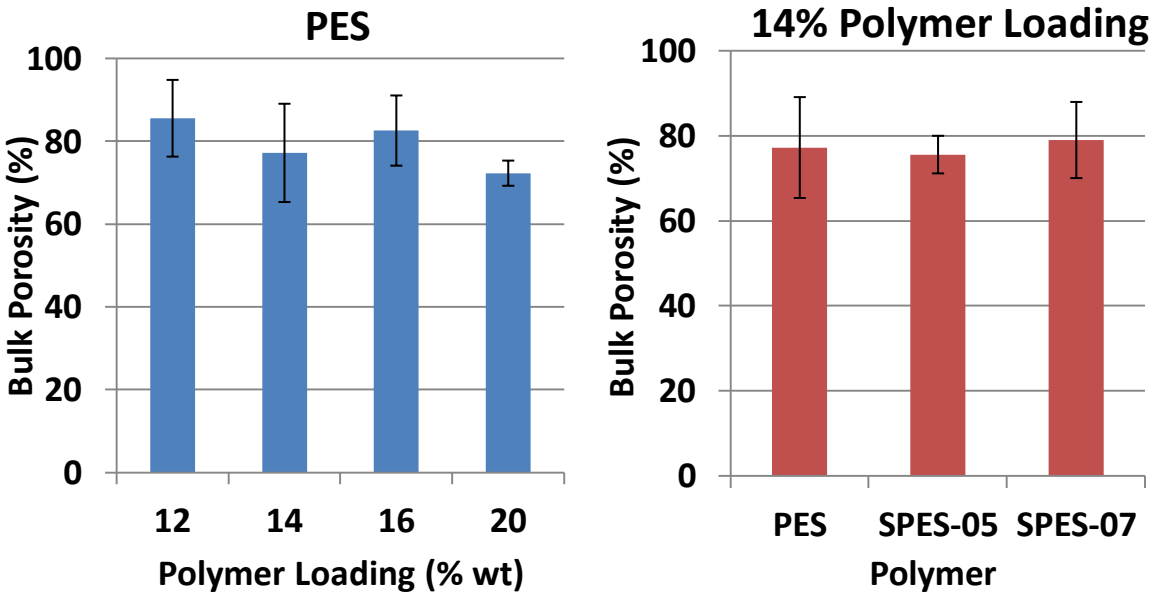

Figure 29: Bulk porosity calculations from MIP data. Porosity as a function of polymer loading (Left) and bulk porosity as a function of sulfonation (Right). Values are the average of three trials.

It was hypothesized that porosity and sulfonation are directly related. From the data that does not appear to be the case. It could, however, be that the sulfonation is resulting in more larger pores on the surface of the membrane. In order for this to be verified, surface porosity data needs to be examined.

6.2. Thin Film Composite

Polyamide layers were successfully fabricated on top of the asymmetric membranes to create TFC membranes from the cross linking of MPD and TMC. The TFC membranes were characterized using Field Emission Scanning Electron Microscopy (FESEM) for pore structure, and reverse osmosis (RO) and forward osmosis (FO) testing for performance.

6.2.1. Polymer Selection for Interfacial Polymerization

Two polymers, SPES-05 and SPES-07 were chosen for interfacial polymerization in addition to PES, which was the control. This was a result of several factors: handling ability, pure water permeability, pore structure, and casting ability. The membranes need to be easy to both cast and handle as much preparation goes into making the composite membranes. Additionally, an ideal pore structure is desired to get maximum performance from the membranes. From the previous data, it was determined that the 14% SPES-05 and SPES-07 possessed all of the requirements for further testing.

6.2.2. SEM of TFC Membranes

The cross-section and top surface images of the TFC membranes can be seen below in Figure 30. The pore structures contain the desired finger-like pores throughout the length of the support in addition to a dense layer near the top surface to support the active layer. The polyamide active layers, seen in the lower images, exhibit the nodular morphology as described by Ghosh et. al [54, 55].

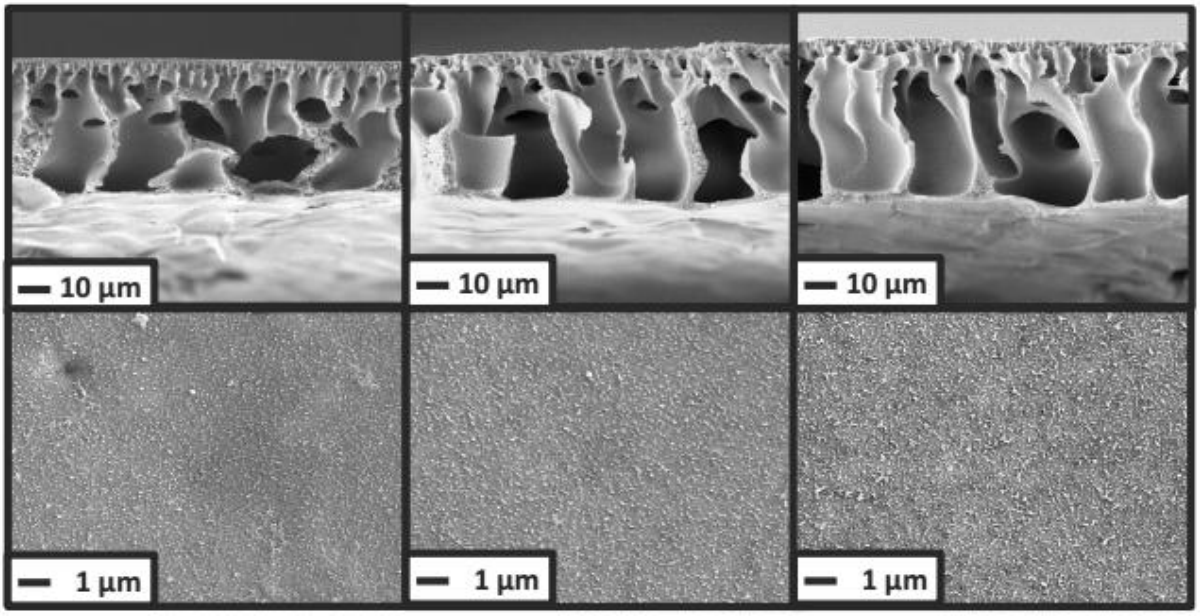

Figure 30: FESEM images of TFC membranes. PES (left), SPES-05 (center), SPES-07 (right).

The active layers appear continuous and as will be seen below, exhibit high salt rejections, indicating that a functional polyamide layer was formed.

6.2.3. Reverse Osmosis Data

As seen below the RO flux of the SPES-05 membranes were on average the highest at just over 5.2 LMH, but negated by the large deviation present in the experimental results.

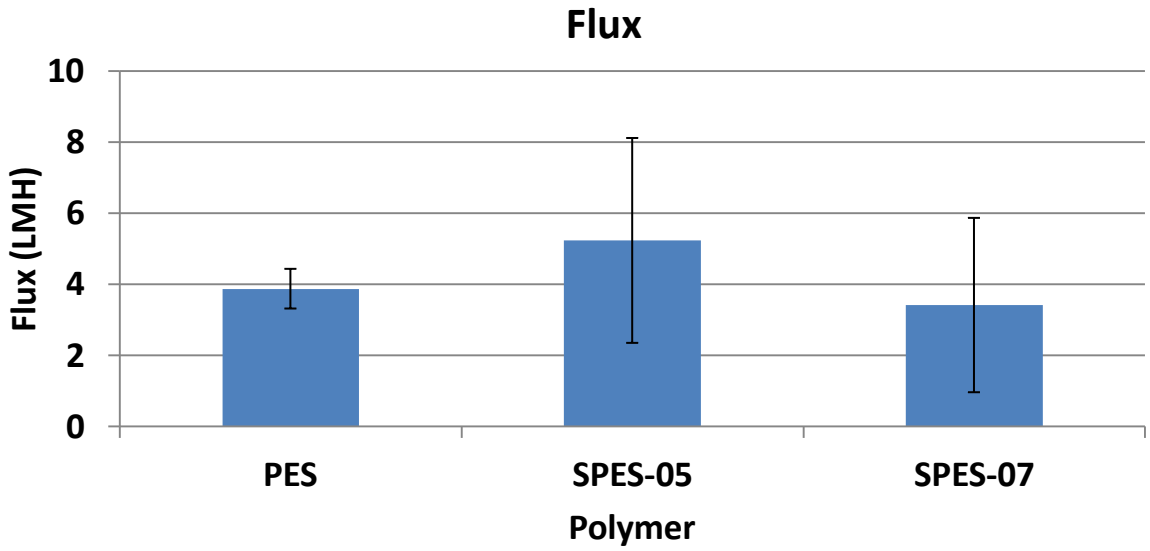

Figure 31: RO flux data. Values are the average of three trials.

The PES and the SPES-07 were just below with 3.9 and 3.5 LMH, respectively. It was previously hypothesized that the sulfonated polymers would result in greater fluxes due to their greater hydrophilicity. In order to verify if there is a statistical difference between the flux values t-Tests were completed using criterion of $p < 0.05$. The t-Tests determined there were no statistically significant differences in the membrane fluxes, therefore failing to support the proposed hypothesis.

Looking at Table 5, the individual permeabilities and salt rejections for the membranes are presented. As expected from the flux data above, SPES-05 had the highest average permeability with 1.18 LMH/Bar, however unverified due to the large deviation. The highest salt rejection however, was seen with the PES membrane at 91.0% and then 88.7% and 84.8% with the SPES-05 and SPES-07, respectively.

Polymer	**Permeability (LMH/Bar)**	**Salt Rejection (%)**	**Salt Permeability (m/s)**
PES	0.395 ± 0.23	91.0 ± 2.3	1.05E-07 ± 2.6E-08
SPES-05	1.18 ± 0.79	88.7 ± 5.9	1.68E-07 ± 8.9E-08
SPES-07	0.974 ± 0.50	84.8 ± 5.1	1.46E-07 ± 7.4E-08

Table 5: Permeability, Salt Rejection and Salt Permeability values for TFC membranes as determined from RO testing.

From the salt permeability, it can be seen that as salt rejection decreases, the salt permeability increases. Overall the lowest salt permeability was seen by the PES membrane, then SPES-07 and SPES-05, one positive aspect is that the salt permeabilities are all of the same order of magnitude, and in fact very little from one another. The SPES-05 salt permeability is the highest due to the larger standard deviation in performance.

Again, the values presented in Table 5 contain large deviations so t-Tests were performed using the same criterion of $p < 0.05$ as done previously. Similarly, there are no statistical difference between the permeabilities and salt rejections of the sulfonated polymers and the control PES.

6.2.4. Forward Osmosis Data

The successfully made TFC membranes were tested in forward osmosis (FO) test systems as discussed previously. The membranes were tested as is, with the PET backing layer intact, and with the PET layer removed. Data was compared to the commercial FO membrane produced by HTI (HTI-CTA). From Figure 32 below it can be seen that fluxes from the TFC membranes were very low, around 2 LMH for the 1.5M NaCl draw solution, whereas the HTI-CTA averaged 15 LMH at the same draw solution concentration.

There are two possible reasons why the TFC membrane did not perform well in FO testing, the first is internal concentration polarization, and the second is membrane wetting. Since there was virtually no performance difference between the three membranes, it was determined that ICP was not the reason for the poor performance, but rather membrane wetting.

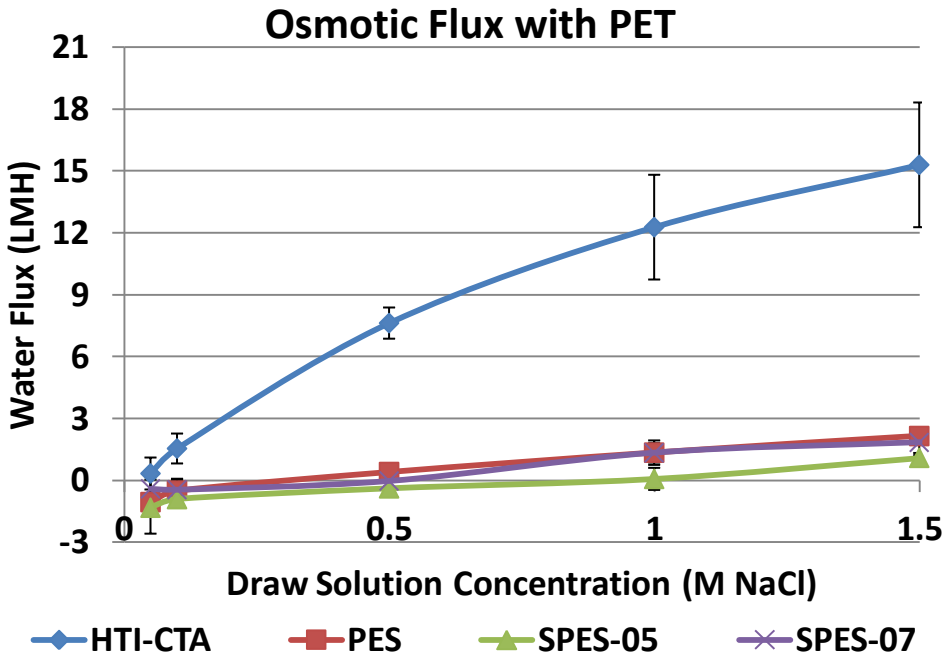

Figure 32: Osmotic flux data with PET layer.

Due to the membranes not fully wetting out during the testing the salts were not able to get close to the active layer in order to create a large concentration gradient to facilitate flux as observed by [14,22]. In order to remediate this issue testing was done after removing the thick PET layer. Membranes that were previously 150-170 µm in thickness were now 40-60 µm thick. In addition, there is significantly less resistance to water flow through the membrane because the membrane are only a third of what they previously were.

The data after removing the PET layer is in Figure 33. The osmotic fluxes increased, especially for the pure PES membrane, which had an average flux about 10 LMH. The sulfonated polymers, SPES-05 and SPES-07 still exhibited low fluxes but they were higher than with the PET layer.

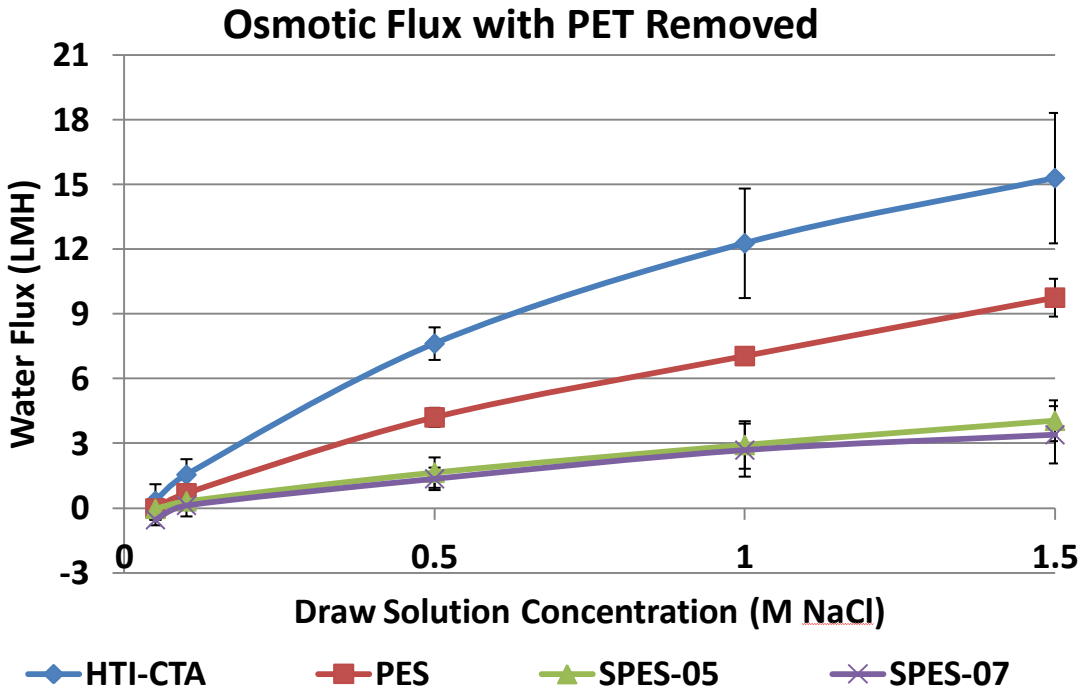

Figure 33: Osmotic flux with PET layer removed.

From the second data set, it can still be seen that wetting is an issue with the TFC membranes made from the sulfonated polymers. A third test was performed, the addition of SDS, a surfactant in order to completely wet out the pore structure of these membranes. This was performed with a draw solution concentration of 1.5 M NaCl, the data can be seen below in Figure 34.

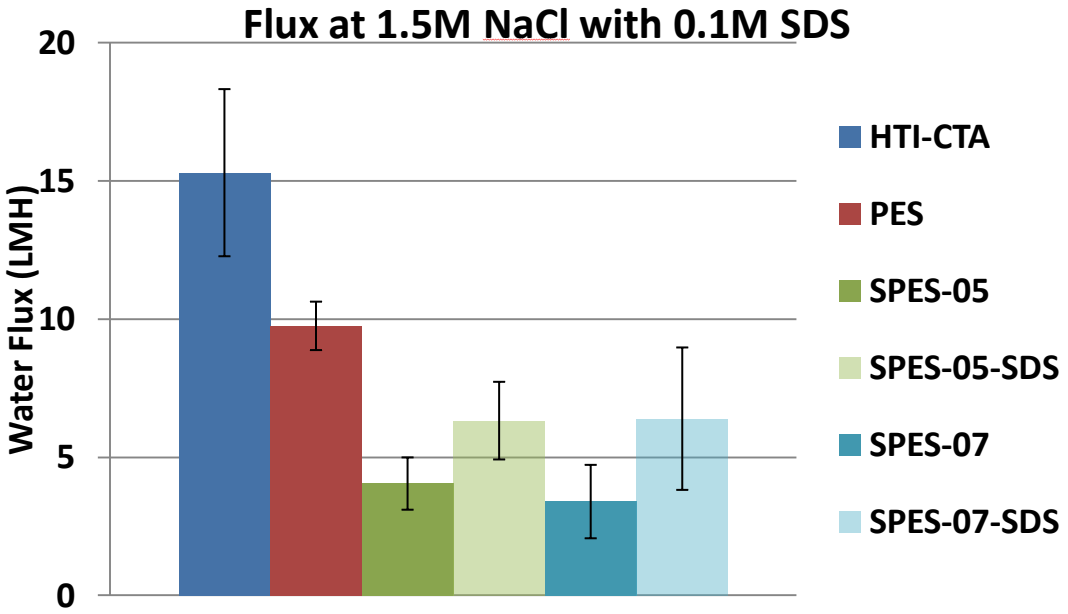

Figure 34: Osmotic flux with 1.5M NaCl draw solution effects of SDS addition.

As can be seen from the graph, the osmotic flux did increase with the addition of SDS. The flux increased by a factor of 1.6 for the SPES-05 and 1.8 for the SPES-07 membranes, respectively. With the addition of the SDS the osmotic flux still falls significantly short of the PES and HTI-CTA performance.

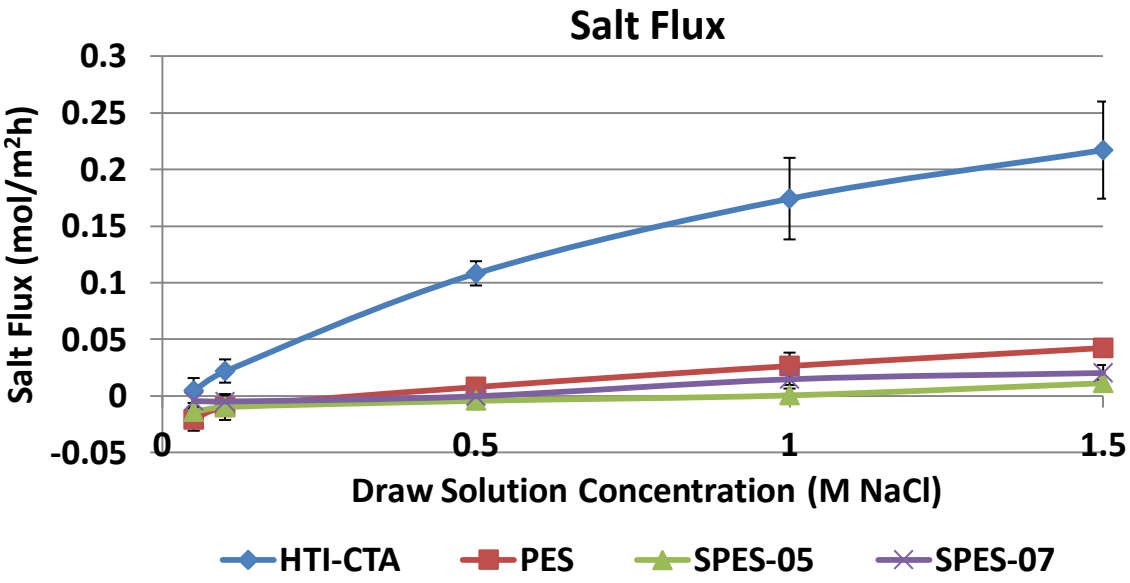

Figure 35: Salt flux of TFC membranes as a function of draw solution concentration.

This low salt flux, since it was present for all of the membranes, further indicates that wetting is an issue for the TFC membranes. After removing the PET layer, the salt flux for the PES membrane increases as depicted in Figure 36. Generally, increased osmotic flux is correlated with increased salt flux [56, 57]. Arena et al. noted that if salts are diffusing out of the support layer with greater ease, they are not residing in the support layer thus resulting in a reduced osmotic driving force [22]. Increased support layer wetting increases both water and salt flux.

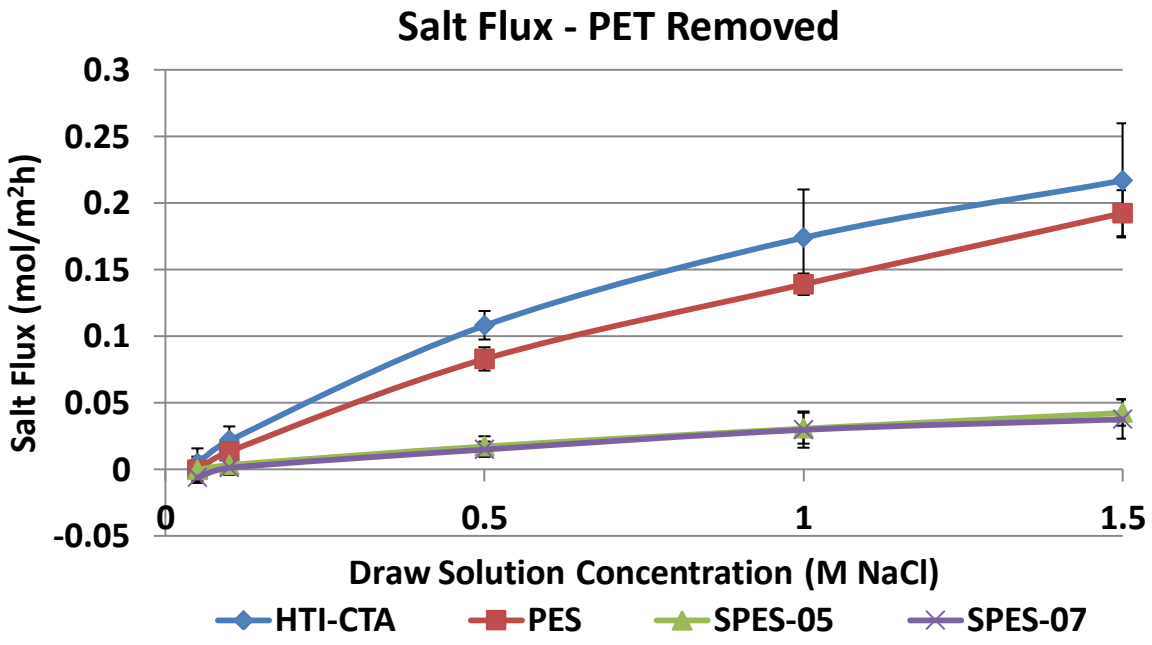

Figure 36: Salt flux of TFC membranes with PET layer removed as a function of draw solution concentration.

Lastly, structural parameters (S) were calculated for the TFC membranes with the PET layer removed by fitting the data from Figure 33 to Equation 6. As was expected, the PES membrane had the lowest S value followed by SPES-05 and SPES-07, which were an order of magnitude greater. The calculated S values for the SPES TFC membranes were significantly higher than the PES due to their poor FO performance, which has been attributed to limited membrane wetting.

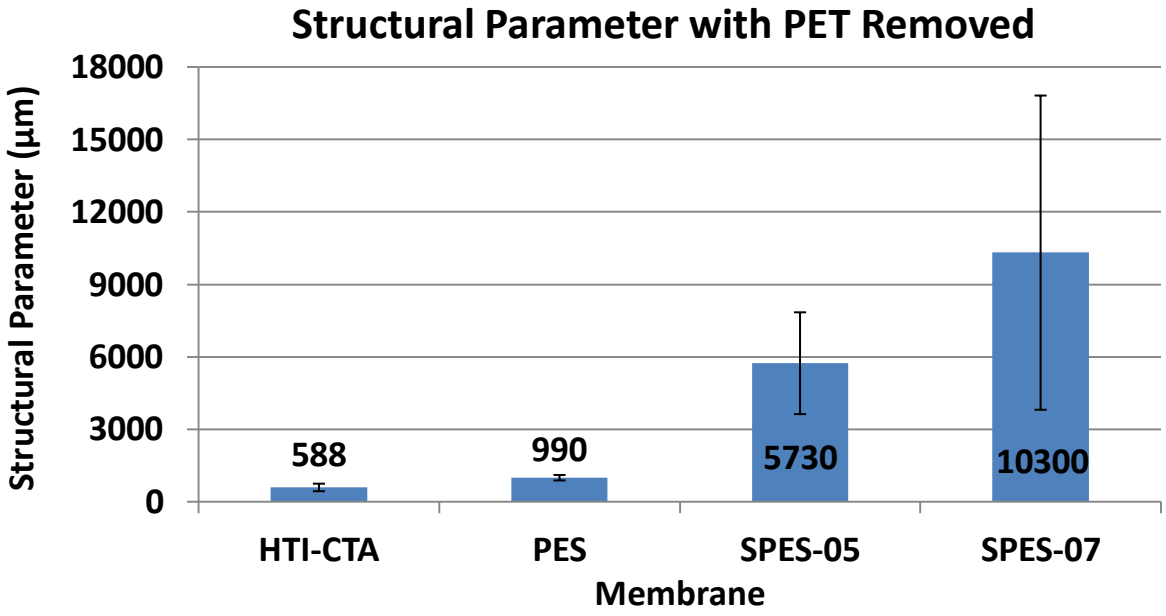

Figure 37: Structural parameter of TFC membranes with PET removed.

Despite the superior performance of the PES TFC membranes, they still suffer from ICP effects, this can be seen from their nonlinear dependence in Figure 33. The S parameter is a good indication of a membrane's ability to minimize ICP effects. Yip et al. describe the S parameter as the characteristic distance a solute particle must travel to reach the active layer of the membrane from the bulk solution [18]. From the data presented, despite a desired pore structure, support layer wetting plays a crucial role in FO performance.

7. Discussion

SPES is a practical new platform for TFC membranes. As shown, the sulfonated polymers are more hydrophilic than the unmodified PES, which results in less resistance to water transport. Looking at the RO performance of the SPES TFC membranes the salt rejection was lower on average than the PES membranes. This is believed to result from either non-uniformities in the polyamide layer or poorer adhesion to the support layer. A non-uniform active layer creates localized fluxes and resistances and this could be from surface morphologies on the support layer. Previously, Ghosh observed that the hydrophilicity of the support layer influences the shape of the meniscus between the aqueous and organic phases

that ultimately form the resulting polyamide [55]. Additionally, the added polarity from the sulfonation reaction could result in poor polyamide adhesion to the membrane support and therefore limited performance; whereas, in the PES membranes, there are no additional side groups to increase polarity and impede polyamide adhesion.

Membrane wetting in FO testing greatly hindered osmotic performance as shown by limited water and salt fluxes. This issue might be remediated by investigating alternative pore structures i.e. spongier with less macrovoids or a combination.

8. Conclusions

TFC membranes were successfully made using sulfonated polyethersulfone as a substrate material. The asymmetric substrates were characterized using a variety of techniques before two polymers were selected for the interfacial polymerization (SPES-05 and SPES-07). A polyamide layer was fabricated upon the membrane substrates and they were tested in RO and FO systems for osmotic flux performance. It was seen in RO testing that the sulfonated polymer based membranes matched the performance of the PES membranes. As a result of large deviations in results, no statistically significant differences were seen between the tested membranes. In FO testing, the PES membrane performed significantly better than the membranes with sulfonated polymers, this was a result of poor membrane wetting.

Overall sulfonated polyethersulfone (SPES) is a suitable polymer for membrane substrates in osmotic separations. It was seen the lower degrees of sulfonation provide improved membrane permeability and due to lower membrane resistance.

9. Future Work

Future work includes a study of surface porosity and its relationship to polymer sulfonation. Secondly, other monomers should be considered for active layer fabrication as the specific surface properties of the films may be better suited for a different chemistry. Furthermore, other process conditions should also be systematically investigated; monomer concentration, monomer solvent, coating times, evaporation times, along with curing times and temperatures.

10. References

[1] R.W. Baker, Membrane Technology and Applications Second Edition. John Wiley & Sons; Hoboken, 2004.

[2] Koch Membrane Systems - 2004

[3] UNESCO. World Water Assessment Program: Facts and Figures. Available at: http://www.unesco.org/water/wwap/facts_fig-ures/. 2009

[4] R.L. McGinnis, M. Elimelech, Global Challenges in Energy and Water Supply: The Promise of Engineered Osmosis, Environmental Science and Technology 42 (2008) 8626-8629.

[5] J.R. McCutcheon, R.L. McGinnis, M. Elimelech, A novel ammonia-carbon dioxide forward (direct) osmosis desalination process, Desalination 175 (2005) 1-11.

[6] S. Loeb, Osmotic power plants, Science 189 (1974) 350.

[7] H.H.G. Jellinek, Osmotic work I. Energy production from osmosis on fresh water/saline water systems, Kagaku Kojo 19 (1975) 87.

[8] S. Loeb, Production of energy from concentrated brine by pressure-retarded osmosis. I. Preliminary technical and economic correlations, Journal of Membrane Science 1 (1976) 49.

[9] G.L. Wick, Energy from salinity gradients, Energy 3 (1978) 95.

[10] J.R. McCutcheon , M. Elimelech, Influence of concentrative and dilutive internal concentration polarization on flux behavior in forward osmosis, Journal of Membrane Science 284 (2006) 237-247.

[11] T.Y. Cath, A.E. Childress, M. Elimelech, Forward osmosis: principles, applications, and recent developments, Journal of Membrane Science 281 (2006) 70–87.

[12] G.T. Gray, J.R. McCutcheon, M. Elimelech, Internal concentration polarization in forward osmosis: role of membrane orientation, Desalination 197 (2006) 1-8.

[13] K.L. Lee, R.W. Baker, H.K. Lonsdale, Membranes for power-generation by pressure-retarded osmosis, Journal of Membrane Science 8 (1981) 141–171.

[14] J.R. McCutcheon, M. Elimelech, Influence of membrane support layer hydrophobicity on water flux in osmotically driven membrane processes, Journal of Membrane Science 318 (2008) 458–466.

[15] Mulder, M, Basic principles of membrane technology, Second Edition, Kluwer Academic, Dordrecht; Boston, 1996.

[16] H.K. Lonsdale, R.L. Riley, C.R. Lyons, D.P. Carosella, Transport in composite reverse osmosis membranes, in:M. Bier (Ed.), Membrane Processes in Industry and Biomedicine, Plenum Press, New York, 1971, pp. 101–122.

[17] J.R. McCutcheon, Resistance profile in TFC membranes, 2012

[18] N.Y. Yip, A. Tiraferri, W.A. Phillip, J.D. Schiffman, M. Elimelech, High performance thin-film composite forward osmosis membrane, Environmental Science and Technology 44 (2010) 3812-3818.

[19] A. Tiraferri, N.Y. Yip, W.A. Phillip, J.D. Schiffman, M. Elimelech, Relating performance of thin-film composite forward osmosis membranes to support layer formation and structure, Journal of Membrane Science 367 (2011) 340-352.

[20] N.-N. Bui, M.L. Lind, E.M.V. Hoek, J.R. McCutcheon, Electrospun nanofiber supported thin film composite membranes for engineered osmosis, Journal of Membrane Science, 385–386 (2011) 10-19.

[21] L. Huang, N.-N. Bui, M.T. Meyering, T.J. Hamlin, J.R. McCutcheon, Novel hydrophilic nylon 6,6 microfiltration membrane supported thin film composite membranes for engineered osmosis, Journal of Membrane Science (*in press*).

[22] J.T. Arena, B. McCloskey, B.D. Freeman, J.R. McCutcheon, Surface modification of thin film composite membranes support layers with polydopamine: enabling use of reverse osmosis membranes in pressure retarded osmosis, Journal of Membrane Science 375 (2011) 55-62.

[23] C.L. Brousse, R. Chapurlat, J.P. Quentin, New membranes for reverse osmosis I. Characteristics of base polymer: sulphonated polysulphones, Desalination 18 (1976) 137-153.

[24] R. Nolte, K. Lodjeff, M. Bauer, R. Mülhaupt, Partially sulfonated poly (arylene ether sulfone) - a versatile proton conducting membrane material for modern energy conversion technologies, Journal of Membrane Science 83 (1993) 211-220.

[25] L. Li, Y. Wang, Sulfonated polyethersulfone cardo membranes for direct methanol fuel cell, Journal of Membrane Science 246 (2005) 167-177.

[26] R. Guan, H. Dai, C. Li, J. Liu, J. Xu, Effect of casting solvent on the morphology and performance of sulfonated polyethersulfone membranes, Journal of Membrane Science 277 (2006) 148-156.

[27] C. Klaysom, B.P. Ladewig, G.Q.M. Lu, L. Wang, Preparation and characterization of sulfonated polyethersulfone for cation-exchange membranes, Journal of Membrane Science 368 (2011) 48-53.

[28] I.C. Kim, J.G. Choi, T.M. Tak, Sulfonated polyethersulfone by heterogeneous method and its membrane performances, Journal of Applied Polymer Science 74 (1999) 2046-2055.

[29] A.K. Ghosh, V. Ramachandhran, M.S. Hanra, B.M. Misra, Synethsis, characterization, and performance of sulfonated polyethersulfone nanofiltration membranes, Journal of Macromolecular Science Part A: Pure and Applied Chemistry 39 (2002) 199-216.

[30] L. Unnikrishnan, S.K. Nayak, S. Mohanty, G. Sarkhel, Polyethersulfone membranes: the effect of sulfonation on the properties, Polymer-Plastic Technology and Engineering 49 (2010) 1419-1427.

[31] W.F.C Kools, Membrane formation by phase inversion in multicomponent polymer systems: mechanisms and morphologies, PhD thesis Chemical Engineering University of Twente (1998).

[32] M.H.V. Mulder, J.O. Hendrikman, J.G. Wijmans, C.A. Smolders, A rationale for the preparation of asymmetric pervaporation membranes, Journal of Applied Polymer Science 30 (1985) 2805–2820.

[33] A.J. McHugh, C.S. Tsay, Dynamics of the phase inversion process, Journal of Applied Polymer Science 46 (1992) 2011–2021.

[34] J.G. Wijmans, J. Kant, M.H.V. Mulder, C.A. Smolders, Phase separations phenomena in solutions of polysulfone in mixtures of a solvent and a nonsolvent: relationship with membrane formation, Polymer 26 (1985) 1539-1545.

[35] L. Yilmaz, A.J. McHugh, Analysis of nonsolvent-solvent-polymer phase diagrams and their relevance to membrane formation modeling, Journal of Applied Polymer Science 31 (1986) 997-1018.

[36] W.W.Y. Lau, M.D. Guiver, T. Matsuura, Phase separation in polysulfone/solvent/water and polyethersulfone/solvent/water systems, Journal of Membrane Science 59 (1991) 219-227.

[37] S.S. Shojaie, Polymeric dense films and membranes via the dry-cast phase -inversion process: modelling, casting, and morphological studies, PhD thesis Chemical Engineering University of Colorado (1992).

[38] C. Cohen, G.B. Tanny, S. Prager, Diffusion-controlled formation of porous structures in ternary polymer systems, Journal of Polymer Science: Polymer Physics Edition 17 (1979) 477-489.

[39] A.J. Reuvers, J.W.A. van den Berg, C.A. Smolders, Formation of membranes by means of immersion precipitation Part I. A model to describe mass transfer during immersion precipitation, Journal of Membrane Science 34 (1987) 45-65.

[40] I. Cabasso, Ultrastructure of asymmetric and composite membranes, ACS Symposium Ser 153 (1981) 267.

[41] C.S. Tsay, A.J. McHugh, Mass transfer modeling of asymmetric membrane formation by phase inversion, Journal of Polymer Science: Part B: Polymer Physics 28 (1990) 1327-1365.

[42] S.S. Shojaie, W.B. Krantz, A.R. Greenberg, Dense polymer films and membrane formation vie the dry cast process part I. Model development, Journal of Membrane Science 94 (1994) 255-280.

[43] P. van de Witte, P.J. Dijkstra, J.W.A. van den Berg, J. Feijen, Phase separation processes in polymer solutions in relation to membrane formation, Journal of Membrane Science 117 (1996) 1–31.

[44] S.A. McKelvey, W.J. Koros, Phase separation, vitrification, and the manifestation of macrovoids in polymeric asymmetric membranes, Journal of Membrane Science 112 (1996) 29–39.

[45] C.A. Smolders, A.J. Reuvers, I.M. Wienk, Microstructures in phase-inversion membranes. Part I. Formation of macrovoids, Journal of Membrane Science 73, (1992) 259-275.

[46] J.G. Wijmans, R.W. Baker, The solution-diffusion model: a review, Journal of Membrane Science, 107 (1995) 1-21.

[47] C.Y. Tang, Y.-N. Kwon, J.O Leckie, Effects of membrane chemistry and coating layer on physiochemical properties of thin film composite polyamide RO and NF membranes I. FTIR and XPS characterization of polyamide and coating layer chemistry, Desalination 242 (2009) 149-167.

[48] S. S Manickam, J.R. McCutcheon, Characterization of polymeric nonwovens using porosimetry, porometry, and x-ray computed tomography, Journal of Membrane Science 407-408 (2012) 108-115.

[49] Micrometrics Instrument Corporation – Mercury Intrusion Porosimetry Theory Poster.

[50] T.Y. Cath, M. Elimelech, J.R. McCutcheon, R.L. McGinnis, A.Achilli, D.Anastasio, A.R. Brady, A.E. Childress, I.V. Farr, N.T.Hancock, J.Lampi, L.D. Ngheim, M.Xie, N.Y. Yip, Standard methodology for evaluating membrane performance in osmotically driven membrane processes, Desalination 312 (20130) 31-38.

[51] R. Guan, H. Zou, D. Lu, C. Gong, Y. Liu, Polyethersulfone sulfonated by chlorosulfonic acid and its membrane characteristics, European Polymer Journal 41 (2005) 1554-1560.

[52] F. Lufrano, G. Squadritto, A. Patti, E. Passalacqua, Sulfonated polysulfone as promising membranes for polymer electrolyte fuel cells, Journal of Applied Polymer Science 77 (2000) 1250-1257.

[53] K.J. Kim, P.V. Stevens, Hydraulic and surface characteristics of membranes with parallel cylindrical pores, Journal of Membrane Science 123 (1997) 303-314.

[54] A.K. Ghosh, B.H. Jeong, X. Huang, E.M.V. Hoek, Impacts of reaction and curing conditions on polyamide composite reverse osmosis membrane properties, Journal of Membrane Science 311 (2008) 34-45.

[55] A.K. Ghosh, E.M.V. Hoek, Impacts of support membrane structure and chem-istry on polyamide–polysulfone interfacial composite membranes, Journal of Membrane Science 336 (2009) 140–148

[56] N.T. Hancock, T.Y. Cath, Solute coupled diffusion in osmotically driven membrane processes, Environmental Science and Technology 43(2009) 6769–6775.

[57] W.A. Phillip, J.S. Yong, M. Elimelech, Reverse draw solute permeation in forward osmosis: modeling and experiments, Environmental Science and Technology 44 (2010) 5170–5176.

[58] P.R. Laity, P.M. Glover, J.N. Hay, Composition and phase changes observed by magnetic resonance imaging during non-solvent induced coagulation of cellulose , Polymer 43 (2002) 5827-5837.